J_ID: PETROLOGY Customer A_ID: EGX073 Copyedited by: PR Manuscript Category: Original Article Cadmus Art: O

Author Query Form

Journal: *Journal of Petrology*
Article Doi: 10.1093/petrology/egx073
Article Title: Geochemical Constraints Provided by the Freetown Layered Complex (Sierra Leone) on the Origin of High-Ti Tholeiitic CAMP Magmas
First Author: Sara Callegaro
Corr. Author: Sara Callegaro

AUTHOR QUERIES – TO BE ANSWERED BY THE CORRESPONDING AUTHOR

The following queries have arisen during the typesetting of your manuscript. Please click on each query number and respond by indicating the change required within the text of the article. If no change is needed please add a note saying "No change."

AQ1: Marzoli et al. 1999 - year not as in reference list. Which reference should this be?

AQ2: Lytwin et al. 2006 - spelling not as in reference list. Which is the correct version? Please make consistent throughout paper

AQ3: Burke & Webb 2003 - please confirm change from Burke et al. is correct

AQ4: 201·7 ± 0·7 [0·8] - please explain meaning of value in square brackets

AQ5: Briden 1977 - please add details to reference list

AQ6: Meisel et al. 2002 - please add details to reference list

AQ7: Burke & Webb 2003 - please confirm change from Burke et al. is correct

AQ8: Carlson et al. 1996 - please confirm change from Carlson 1996, here and later in text, is correct. If not, please add details of Carlson 1996 to reference list

AQ9: Callegaro et al. 2014 - please give first three authors before 'et al.'

AQ10: Comin-Chiaramonti et al. 2007 - please give only one page range for the paper

AQ11: Gao et al. 2008 - please give first three authors' names before 'et al.', and add journal title

AQ12: Hargraves et al. 1999 - please complete the paper title

AQ13: Hofmann 2003 - please confirm added publisher is correct

AQ14: Marzoli et al. 2011 - please give first three authors' names before 'et al.'

AQ15: Merle et al. 2014 - please give first three authors' names before 'et al.'

AQ16: Nowell et al. 2003 - please add volume number

AQ17: Svensen et al. 2017 - please update (add page numbers) if possible

AQ18: Tibbetts 2010 - please give name of university and title of degree

AQ19: I have amended layout of table so that it will fit page area. I hope this is acceptable

AQ20: Fig. 9 caption - Jacobsen & Wasserburg 1980 - please add details to reference list

AQ21: Fig. 13 - should OIB be labelled in figure?

AQ22: Please check that all names have been spelled correctly and appear in the correct order. Please also check that all initials are present. Please check that the author surnames (family name) have been correctly identified by a pink background. If this is incorrect, please identify the full surname of the relevant authors. Occasionally, the distinction between surnames and forenames can be ambiguous, and this is to ensure that the authors' full surnames and forenames are tagged correctly, for accurate indexing online. Please also check all author affiliations.

NOT FOR PUBLIC RELEASE

MAKING CORRECTIONS TO YOUR PROOF

These instructions show you how to mark changes or add notes to your proofs using Adobe Acrobat Professional versions 7 and onwards, or Adobe Reader DC. To check what version you are using go to **Help** then **About**. The latest version of Adobe Reader is available for free from get.adobe.com/reader.

DISPLAYING THE TOOLBARS

Adobe Reader DC

In Adobe Reader DC, the Comment toolbar can be found by clicking 'Comment' in the menu on the right-hand side of the page (shown below).

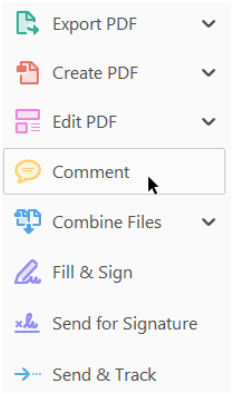

The toolbar shown below will then display along the top.

Acrobat Professional 7, 8, and 9

In Adobe Professional, the Comment toolbar can be found by clicking 'Comment(s)' in the top toolbar, and then clicking 'Show Comment & Markup Toolbar' (shown below).

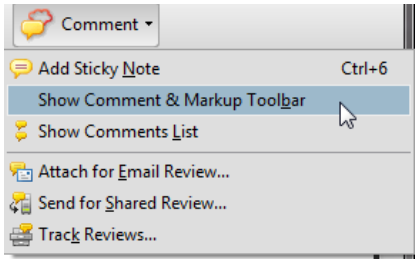

The toolbar shown below will then be displayed along the top.

USING TEXT EDITS AND COMMENTS IN ACROBAT

This is the quickest, simplest and easiest method both to make corrections, and for your corrections to be transferred and checked.

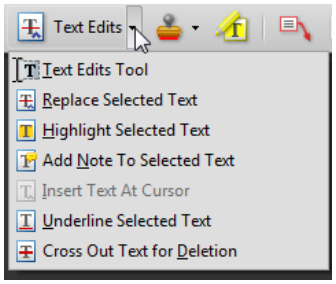

1. Click **Text Edits**
2. Select the text to be annotated or place your cursor at the insertion point and start typing.
3. Click the **Text Edits** drop down arrow and select the required action.

You can also right click on selected text for a range of commenting options, or add sticky notes.

SAVING COMMENTS

In order to save your comments and notes, you need to save the file (**File, Save**) when you close the document.

USING COMMENTING TOOLS IN ADOBE READER

All commenting tools are displayed in the toolbar. You cannot use text edits, however you can still use highlighter, sticky notes, and a variety of insert/replace text options.

POP-UP NOTES

In both Reader and Acrobat, when you insert or edit text a pop-up box will appear. In **Acrobat** it looks like this:

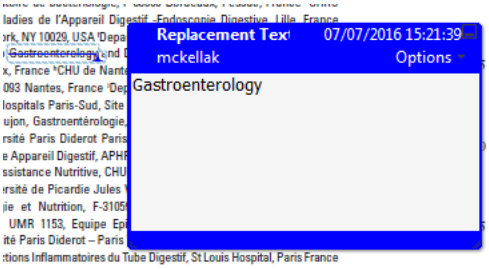

In **Reader** it looks like this, and will appear in the right-hand pane:

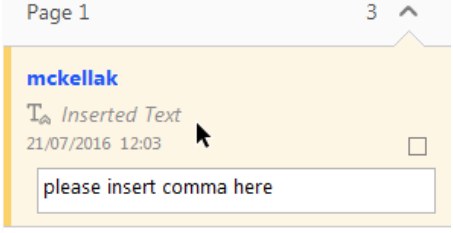

DO NOT MAKE ANY EDITS DIRECTLY INTO THE TEXT, USE COMMENTING TOOLS ONLY.

J_ID: PETROLOGY Customer A_ID: EGX073 Copyedited by: PR Manuscript Category: Original Article Cadmus Art: O

JOURNAL OF PETROLOGY

Journal of Petrology, 2017, 1–28
doi: 10.1093/petrology/egx073
Original Article

OXFORD

Geochemical Constraints Provided by the Freetown Layered Complex (Sierra Leone) on the Origin of High-Ti Tholeiitic CAMP Magmas

Sara Callegaro[1,2]*, Andrea Marzoli[2,3], Hervé Bertrand[4], Janne Blichert-Toft[4], Laurie Reisberg[5], Giancarlo Cavazzini[3], Fred Jourdan[6], Joshua Davies[7], Laura Parisio[2], Romain Bouchet[4], Andre Paul[7], Urs Schaltegger[7] and Massimo Chiaradia[7]

[1]Centre for Earth Evolution and Dynamics (CEED), University of Oslo, PO Box 1028, Blindern, N-0316 Oslo, Norway; [2]Dipartimento di Geoscienze, Università di Padova, via Gradenigo 6, 35131 Padova, Italy; [3]Istituto di Geoscienze e Georisorse, C.N.R., Via Gradenigo 6, 35131 Padova, Italy; [4]Laboratoire de Géologie de Lyon, Université Lyon 1 and Ecole Normale Supérieure de Lyon, UMR CNRS 5276, 46 Allée d'Italie, 69364 Lyon Cedex 7, France; [5]Centre de Recherches Pétrographiques et Géochimiques, UMR 7358 CNRS, Université de Lorraine, BP 20, 54501 Vandoeuvre-les-Nancy Cedex, France; [6]Department of Applied Geology, Curtin University, Bentley, WA 6102, Australia; [7]Section des Sciences de la Terre, Université de Genève, 13 Rue des Maraîchers, 1205 Genève 4, Switzerland

*Corresponding author. E-mail: sara.callegaro@geo.uio.no

Received January 13, 2017; Accepted November 16, 2017

ABSTRACT

The Freetown Layered Complex (FLC) is a massive mafic layered intrusion cropping out along the Atlantic coast of Sierra Leone. The present combined geochemical and geochronological ($^{40}Ar/^{39}Ar$ on plagioclase: 201·7 ± 0·7 and 202·3 ± 2·3 Ma; U–Pb on baddeleyite: 198·794 ± 0·048/0·071/0·22 Ma) study of the complex flags it as a high-Ti occurrence of the Central Atlantic Magmatic Province (CAMP). Sr–Nd–Pb–Os isotope data indicate that the FLC is unique with respect to previously studied CAMP occurrences, constituting a new isotopic end-member for this large igneous province (LIP). Notably, the contribution of ancient source(s) is required to explain its low $^{206}Pb/^{204}Pb$ and high $^{207}Pb/^{204}Pb$. Although the internal isotopic variability of the FLC can be explained by modest assimilation (<10%) of lower crustal (granulitic) material, represented by a xenolith found within the complex itself, an atypical mantle source is required to account for its unusual Pb isotopic composition. We present the first Hf isotopic data measured to date for the CAMP, which, in the case of the FLC, show a restricted range in $^{176}Hf/^{177}Hf$, overlapping the ocean island basalt and mid-ocean ridge basalt fields on the terrestrial array, and can further be used to characterize the FLC isotopic end-member. We propose that the FLC formed by mixing of a predominantly asthenospheric parental magma with small volumes (1–3%) of geochemically highly enriched lamproitic melts derived from the sub-continental lithospheric mantle in a geodynamic context in which a Proterozoic mobile belt (Rokelide) bordered an Archean craton (Man). Within the CAMP, similar isotopic compositions, in particular low $^{206}Pb/^{204}Pb$ and high $^{207}Pb/^{204}Pb$, are found only in regions that were once contiguous with Sierra Leone. A comparable involvement of enriched components stored within the cratonic lithosphere may be envisaged for the high-Ti magmatism in the CAMP and two other LIPs of the South Atlantic realm, Karoo and Paraná–Etendeka. These Gondwana magmatic provinces share with other mantle-derived magmas from the South Atlantic Ocean enriched isotopic signatures (DUPAL, LOMU, EMI) of much debated origin. The present mantle source model for the FLC, CAMP, and neighbouring LIPs suggests ancient enriched subcontinental

J_ID: PETROLOGY Customer A_ID: EGX073 Copyedited by: PR Manuscript Category: Original Article Cadmus Art: O

lithospheric mantle as a plausible conveyor of such isotopic signatures in the South and Central Atlantic.

Key words: CAMP; Freetown Complex; high-Ti tholeiite; layered intrusion

INTRODUCTION

Trace element and isotopic signatures reflecting incompatible element enrichment are observed in both intra-plate igneous rocks (ocean island basalts; OIB) and continental large igneous provinces (LIP), and, to a lesser extent, in mid-ocean ridge basalts (MORB). Recycled lithospheric material, stored in either the deep (e.g. Korenaga, 2004) or the shallow (e.g. Lustrino, 2005) mantle, is often thought to be responsible for these geochemical characteristics (Gao *et al.*, 2008). The Atlantic domain is particularly suitable for the study of such mantle enrichment processes (O'Reilly *et al.*, 2009) owing to the occurrence of enriched oceanic basalts and LIPs associated with the opening of the Atlantic Ocean.

A striking example is the Central Atlantic Magmatic Province (CAMP; Fig. 1a) with peak activity at *c.* 201 Ma (Marzoli *et al.*, 2011; Blackburn *et al.*, 2013; Davies *et al.*, 2017). The CAMP is possibly the largest known igneous province, with relics spread over an area in excess of 10^7 km^2, and is related to the early breakup of Pangea. The vast majority of the CAMP consists of extrusive or shallow intrusive rocks (dykes and sills), but it also includes two major intrusions, specifically the low-Ti Kakoulima laccolith (Guinea; Deckart *et al.*, 1997, 2005) and the Freetown Layered Complex (FLC; Sierra Leone, Chalokwu *et al.*, 1999; Chalokwu, 2001). We here present the first comprehensive geochronological (^{40}Ar/^{39}Ar and U–Pb) and isotopic tracer (Sr–Nd–Hf–Pb–Os) study of the FLC, which includes the first Hf isotopic compositions determined on CAMP rocks. The results of our geochemical study provide new insights on the age and petrogenesis of this igneous complex and possible answers to some longstanding questions about the CAMP in particular and LIPs in general, such as the reason for the paucity and narrow areal extent of high-Ti magmatism and the origin of the enriched signatures commonly associated with magmatism in the South Atlantic region.

THE FREETOWN LAYERED COMPLEX: PREVIOUS STUDIES AND GEOLOGICAL CONTEXT

The Freetown Layered Complex (Fig. 1) in Sierra Leone is a *c.* 6 × 10^3 km^3 mafic layered lopolith (Wells, 1962) emplaced during the early stages of Pangea breakup. The subaerial section of the complex covers 65 × 14 × 7 km along the Atlantic coast, from Freetown to Banana Island, where geophysical surveys reveal it to extend for another 45 km offshore (Krause, 1963; Mgbatogu *et al.*, 1988). Based on topographic (escarpments) and mineralogical observations (rhythmic recurrence of rock types), the FLC has been subdivided into four zones, previously interpreted to mark the injection of different batches of magma into the chamber (Fig. 1b; zones 1–4 in ascending order from east to west; Hattori *et al.*, 1991; Chalokwu *et al.*, 1995, 1999). The presence of supposedly CAMP-related basaltic and doleritic xenoliths in Jurassic kimberlites from Sierra Leone (Koidu and Tong localities, 250 km to the east of the FLC) suggests that the FLC magmas potentially fed rather extensive lava flows and dyke swarms (Skinner *et al.*, 2004). The FLC is cut by roughly coeval coast-parallel fine-grained doleritic dykes, previously interpreted as evolved liquids expelled from the roof zone of the complex in response to convection (Chalokwu, 2001). However, these dykes are part of a CAMP-related basaltic dyke swarm that extends beyond the FLC along the coasts of central–western Africa (from Liberia to Sierra Leone; Dupuy *et al.*, 1988; Mauche *et al.*, 1989) and northeastern South America (from Brazil to Suriname; Deckart *et al.*, 1997, 2005; Marzoli *et al.*, 1999; De Min *et al.*, 2003).

In Sierra Leone, the late Archean basement [~2·7 Ga; composed of granulites, amphibolites, and tonalite–trondhjemite–granodiorite (TTG) gneisses] is part of the West African Craton (locally defined also as the Man Craton), which is bordered to the west by the Rokelides mountains, a coastal orogen formed in the late Proterozoic (Pan African ~; 550 Ma; Lytwin *et al.*, 2006). Lithospheric roots with high seismic velocities are observed as deep as 400 km under Sierra Leone (O'Reilly *et al.*, 2009).

The FLC intruded at mid-crustal depths within the metamorphic terranes of the Kasila Group, part of the Rokelide orogenic belt (2·8–5·1 kbar; Chalokwu *et al.*, 1999). The Kasila Group rocks are dominantly mafic gneisses with minor sedimentary rocks, gabbros and gabbro–anorthosites, poly-metamorphosed in granulite to amphibolite facies. They were metamorphosed first during the late Archean (2·7 Ga) and again during the Pan-African orogeny (*c.* 550 Ma; Lytwin *et al.*, 2006). Therefore, the Rokelide Proterozoic mobile belt that serves as the emplacement site for the FLC has recorded the Neoproterozoic to Early Cambrian oceanic closure and final assembly of Gondwana. This area also witnessed the later opening of the Central Atlantic Ocean that marks the breakup of the Pangaea supercontinent, and thus has experienced (at least) one entire Wilson cycle. The coastal area is partially covered by Cenozoic sediments of the Bullom Series. Notably, both the West African Craton and the Proterozoic sutures in Sierra Leone, Guinea and Liberia are punctuated by alkaline magmatic suites of various compositions (kimberlitic, lamproitic, carbonatitic and nephelinitic) and ages (Proterozoic to Cretaceous; Taylor *et al.*, 1994; Burke & Webb, 2003; Pouclet *et al.*, 2004; Skinner *et al.*, 2004).

J_ID: PETROLOGY Customer A_ID: EGX073 Copyedited by: PR Manuscript Category: Original Article Cadmus Art: O

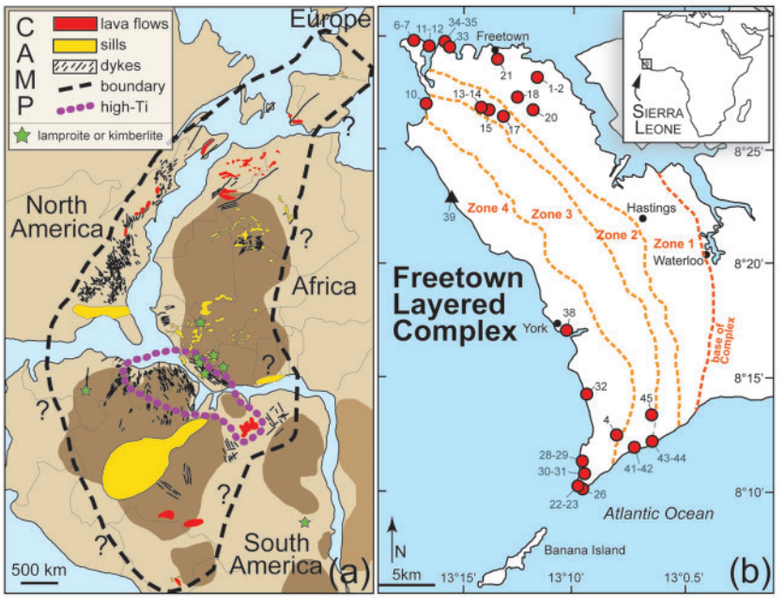

Fig. 1. (a) Outcrops and inferred original limits of the Central Atlantic Magmatic Province shown on a Late Triassic reconstruction of Pangea. ~~Thick violet dotted~~ line contours the areal distribution of high-Ti CAMP rocks. Cratonic areas and kimberlite localities (stars) are indicated. (b) Sampling sites for the FLC rocks, marked with circles for intrusive samples and a black triangle for the dolerite dyke. Dashed lines indicate zone boundaries as reported by Chalokwu *et al.* (1999). The Freetown Layered Complex includes the entire Freetown peninsula as far east as Waterloo (see dashed line marking base of Zone 1) and extends into the ocean for 45 km (Krause, 1963; Mgbatogu *et al.*, 1988).

SAMPLING AND PETROGRAPHY

The FLC was sampled along the coast (Fig. 2a and b), in quarries (Fig. 2c) and in creeks (Fig. 2d), ~~the only~~ localities providing good outcrops free from forest cover. Selective alteration (Fig. 2e) allowed collection of surprisingly fresh samples. Several textural features are visible at the outcrop and hand-sample scale, such as grain-size variations, modal layering, magma mingling textures, and pegmatitic pockets (Fig. 2f–h). The base of the complex was not observed during the field campaign, and the bases of the individual zones were not clearly visible in the field. We observed olivine-, pyroxene-, and plagioclase-rich layers, but no oxide-rich layers, nor were any chilled zones present in the studied outcrops. Dykes were observed in all the zones, both low and high in the intrusion. The contacts between the dykes and the intrusion are all sharp, implying that the intrusion was already crystallized when the dykes cut through it. Unfortunately, difficulties during the field campaign led to loss of all but one dyke sample.

At the thin-section scale, the FLC rocks are fine- to coarse-grained, with a holocrystalline, idiomorphic to hypidiomorphic granular texture, typical of intrusive igneous rocks of mafic composition (Fig. 3). Poikilitic and ophitic textures are observed, and crystals range in size from less than 1 mm to 10 mm. The mineral assemblage is dominated by variable proportions of olivine (20–80%), plagioclase (20–90%), high- and low-Ca clinopyroxene, orthopyroxene (5–60%) and minor oxides, classifying the FLC samples mostly as gabbronorites, olivine gabbros, troctolites and gabbros, with minor occurrences of anorthosite. Olivine crystals are mostly anhedral. In a few cases, they include small opaque minerals and are rimmed by orthopyroxene; occasionally they are partly altered. Plagioclase is mostly euhedral and varies in size from very coarse- to fine-grained. Clinopyroxene crystals are always anhedral, and often show exsolution of low-Ca clinopyroxene and orthopyroxene. Orthopyroxene occurs as anhedral crystals and often rims olivine or augite grains. Oxides are present in all collected samples and vary in size from very small (euhedral) to large (anhedral). Sulphides are generally absent or very rare.

One sample, SL18, an olivine gabbro-norite collected from Zone 1 of the FLC, is markedly different from the other samples. SL18 comprises two parts with distinct mineral proportions~~, with one~~ (~~hereafter~~ SL18N) ~~being~~ olivine-free and dominated by poikilitic orthopyroxene that encloses smaller randomly oriented plagioclase crystals, whereas the other (~~hereafter~~ SL18G) is more typically gabbroic, with few olivine crystals and large augites and plagioclase (Fig. 3). The only available sample from a cross-cutting dyke (SL39) has the typical fine-grained texture of a dolerite, dominated by plagioclase and clinopyroxene. Within the dyke, the primary magmatic phases are partially replaced by secondary amphibole, chlorite, and sericite. For additional petrographic details of the FLC rocks, the interested reader is referred to Umeji (1983) and Chalokwu *et al.* (1995).

J_ID: PETROLOGY Customer A_ID: EGX073 Copyedited by: PR Manuscript Category: Original Article Cadmus Art: O

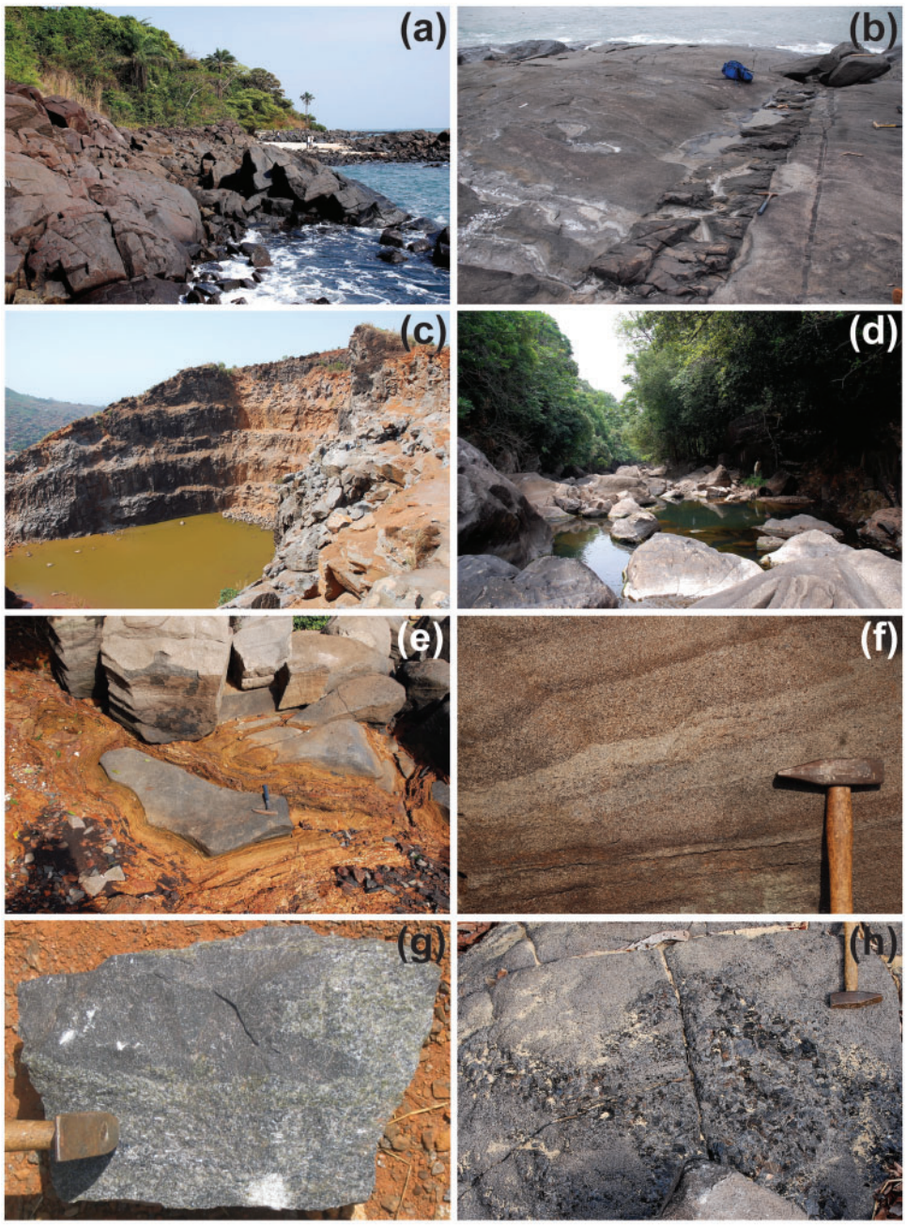

Fig. 2. Field photographs from Sierra Leone. (a, b) Representative outcrops along the shore (a, 8°10·28′N, 13°09·74′W, sample SL26; b, 8°23·12′N, 13°15·82′W). One of the dolerite dykes (SL39) cutting through the complex is visible in (b). (c, d) The complex on land mostly crops out in quarries (c, 8°28·15′N, 13°12·16′W, samples SL1 and SL2) and along streams (d, 8°17·18′N, 13°9·46′W). (e) Selective alteration showing the good preservation of rock cores (8°29·63′N, 13°16·56′W). (f) An example of modal layering (8°29·63′N, 13°16·56′W). (g) Magma mingling visible at the hand-sample scale. (h) Pegmatitic levels (8°14·41′N, 13°09·79′W, sample SL32).

METHODS

Full descriptions of the analytical techniques used for major and trace element concentration determinations in whole-rocks and minerals [by X-ray fluorescence (XRF), electron microprobe analysis (EMPA) and inductively coupled plasma mass spectrometry (ICP-MS)] and for geochronology and radiogenic isotope ratio measurements [Sr–Nd–Pb–Hf–Os by either thermal ionization mass spectrometry (TIMS) or multicollector (MC)-ICP-MS] are included in the Supplementary Data along with the data tables (supplementary data are available for downloading at http://www.petrology.oxfordjournals.org).

GEOCHRONOLOGY OF THE ~~FREETOWN COMPLEX~~

$^{40}Ar/^{39}Ar$ geochronology

The FLC was previously dated at 165 ± 10, 172 ± 8 and 194 ± 8 Ma by Briden *et al.* (1971) based on K–Ar whole-rock analyses and at 199·6 ± 3 Ma by Beckinsale *et al.*

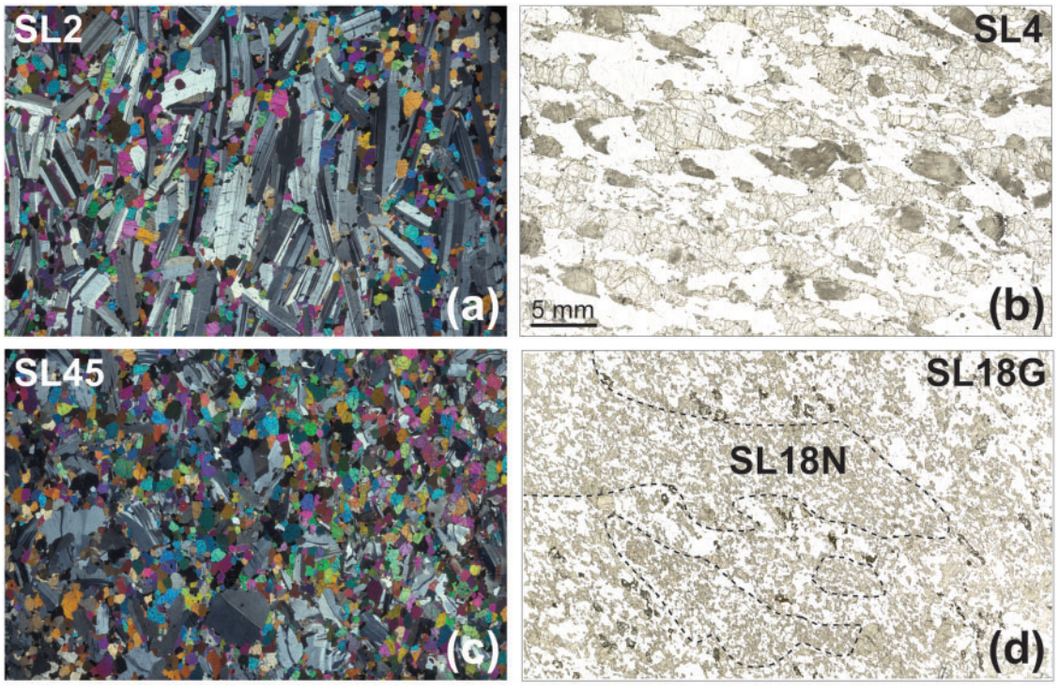

Fig. 3. Photomicrographs (crossed and parallel polars) of some representative rocks from the Freetown Layered Complex. (a) The gabbroic sample SL2 shows preferential orientation of coarse-grained plagioclase laths, along with smaller interstitial olivine and minor pyroxene crystals. (b) The coarse-grained gabbro-norite SL4 shows some preferential orientation of the mafic phases. (c) The olivine gabbro SL45 shows a typical hypidiomorphic granular texture. (d) Sample SL18 shows noritic domains with poikilitic orthopyroxene (SL18N) and gabbroic domains (SL18G), more similar to the other FLC samples. Scale reported in SL4 is valid for all the photomicrographs. (a) and (c), crossed polarized light; (b) and (d), plane-polarized light.

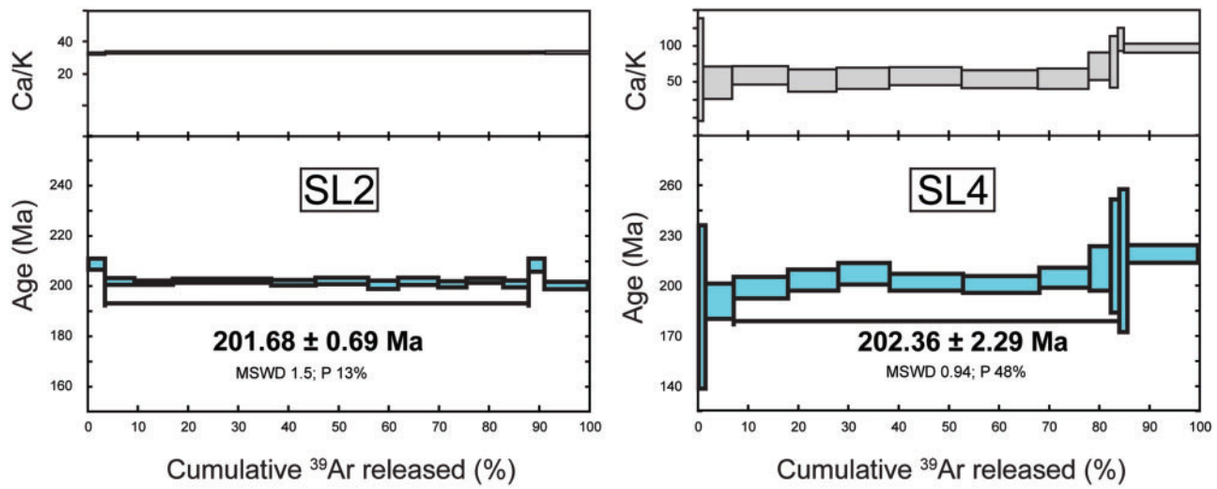

Fig. 4. ^{40}Ar/^{39}Ar age spectra and Ca/K profiles (calculated from ^{37}Ar/^{39}Ar) for samples SL2 and SL4. Errors are shown at the 2σ level. Black horizontal line marks steps included in the plateau age. MSWD, mean square weighted deviation; P, probability. (See Supplementary Data and Supplementary Fig. 1 for further analytical details.)

(1977) [recalculated using the updated decay constant of Rotenberg *et al.* (2012)] based on a whole-rock Rb–Sr isochron for a gabbro–granophyre from Banana Island (Fig. 1). We obtained two ^{40}Ar/^{39}Ar plateau ages (Fig. 4) on plagioclase separates from samples SL2 (noritic troctolite, Zone 1) and SL4 (gabbro, Zone 4) of, respectively, 201·7 ± 0·7 [0·8] Ma and 202·4 ± 2·3 [2·3] Ma. Step-heating of SL2 plagioclase resulted in a robust plateau with 11 concordant steps summing up to 84% released gas (^{39}Ar). The $[Ca/K]_{Ar}$ spectrum (calculated from ^{37}Ar/^{39}Ar) is flat and consistent with the EMP compositions of SL2 analysed crystals ($[Ca/K]_{Ar}$ 30, $[Ca/K]_{EMP}$ 23–33; Fig. 4; Supplementary Data Fig. 1), suggesting that the analysed plagioclase separate was not altered. The inverse isochron yields an age of 201·64 ± 0·88 Ma (Supplementary Data Table 1) concordant with the plateau

age. The initial intercept $^{40}Ar/^{36}Ar$ ratio of 326 ± 64 rules out the presence of excess ^{40}Ar* (radiogenic ^{40}Ar).

The plagioclase separate from SL4 yielded a plateau age defined by 78% released ^{39}Ar and nine consecutive concordant steps, although with a rather large analytical error owing to a relatively high and variable $[Ca/K]_{Ar}$ of 40–100 (Fig. 4). The $[Ca/K]_{Ar}$ ratio from the lower-temperature steps is consistent with the composition of plagioclase phenocrysts ($[Ca/K]_{EMP}$ ranging between 36 and 51; Supplementary Data Fig. 1), whereas the high-temperature steps yielded $[Ca/K]_{Ar}$ clearly higher than those measured with the EMP, suggesting that some crystals may contain high-An cores (e.g. Marzoli *et al.*, 2011). The inverse isochron (Supplementary Data Table 2) yields an age of 200·5 ± 4·3 Ma and is thus in agreement with the plateau age. The possible presence of excess argon, to be expected in a large, rather deep intrusion, cannot be verified with the inverse isochron initial intercept as the value ($^{40}Ar/^{36}Ar = 730 \pm 655$) is poorly defined owing to clustering of all the data at near-constant and low $^{36}Ar/^{40}Ar$. Although the age spectrum of SL4 does not present a clear saddle shape, the highest-temperature steps yield slightly older apparent ages, potentially reflecting excess ^{40}Ar*.

U–Pb geochronology

Only one sample (SL18G) from the FLC yielded dateable baddeleyite (ZrO_2) and apatite. With the use of an optical microscope, 11 large, anhedral, clear, and inclusion-free baddeleyite fragments were selected for dissolution from this sample. All of the grains produced concordant analyses clustering around 198 Ma, with three analyses producing slightly younger ages, most probably owing to open-system behaviour, and one yielding a slightly older age, possibly representing a baddeleyite antecryst. A $^{206}Pb/^{238}U$ weighted mean age for the seven oldest grains (without the older potential antecryst) is 198·777 ± 0·047/0·07/0·22 Ma with an MSWD of 2·3 (Fig. 5; Supplementary Data Fig. 2; Supplementary Data Table 3). The age is presented as $\pm X/Y/Z$ where X represents the internal error, Y the tracer calibration uncertainty plus the internal error, and Z the decay constant uncertainties plus the tracer and internal uncertainties. Baddeleyite grains commonly display minor Pb open-system behaviour, which cannot be removed by chemical abrasion as is often done for zircon (Rioux *et al.*, 2010).

To constrain further the age of the FLC, and sample SL18G, seven subhedral to anhedral, inclusion- and crack-free single apatite grains were handpicked for U–Pb analysis (Supplementary Data Table 3). The apatites range in age from 205 ± 1·5 Ma to 194·49 ± 0·26, with all grains being concordant to slightly discordant, suggesting partial open-system behaviour. Apatite has a Pb closure temperature (T_c) of 350–450 °C, which was calculated using the diffusion coefficient and activation energy of Cherniak (2010) for apatites of Durango composition and the Dodson equation for T_c (Dodson, 1973). All apatite analyses were corrected for common

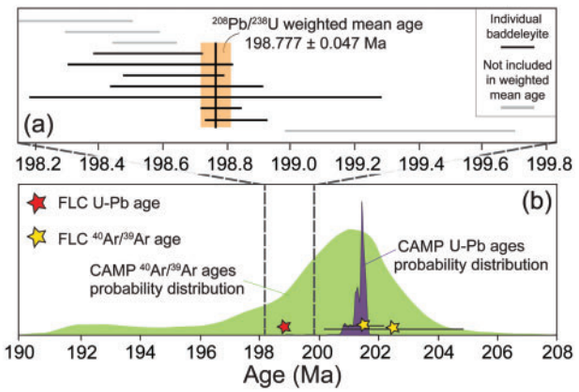

Fig. 5. ~~Upper panel:~~ U/Pb ages obtained from a baddeleyite separate from sample SL18G. Each bar represents a single baddeleyite 2σ uncertainty. Light grey bars reflect analyses not included in the weighted mean age. Age bar for sample SL18_b13 is shown only partially because of its large uncertainty; the age is not included in the weighted mean, as it is the youngest grain and is considered to have experienced Pb open-system behaviour. ~~Lower panel:~~ U–Pb and $^{40}Ar/^{39}Ar$ ages of the FLC plotted on an age probability curve ($^{40}Ar/^{39}Ar$ plateau ages) for the CAMP activity (see Marzoli *et al.*, 2011) along with previously published U–Pb CAMP ages (purple probability density curve; Schoene *et al.*, 2010; Blackburn *et al.*, 2013; Davies *et al.*, 2017).

Pb (Pbc) using $^{206}Pb/^{204}Pb$ and $^{207}Pb/^{204}Pb$ compositions of 17·72 and 15·549, respectively, constrained by a plagioclase analysis from the same sample. As shown below, this initial Pb isotope composition is very similar to those of other rocks ~~of~~ the FLC, supporting the suggestion that the gabbroic portion of sample SL18 is indeed representative of the complex and thus provides pertinent age constraints.

To assist in understanding the apatite U–Pb dates, the trace element contents of the dated apatites were measured following the approach of Schoene *et al.* (2010) for zircon U–Pb and trace element analysis (TIMS-TEA). The apatites show enrichments in light rare earth elements (LREE), a strong negative Eu anomaly, and depleted heavy REE (HREE) (Supplementary Data Fig. 3; Supplementary Data Table 3). The apatites that give young (<199 Ma) U–Pb ages are significantly more U-rich than those yielding old ages (Supplementary Data Fig. 4). All the apatites display a narrow range in Th/U from 4·28 to 5·59, but have variable La/Yb (12·4–32·4), the latter correlating with the age of the grains.

MINERAL CHEMISTRY

Major element data for olivine, pyroxene, plagioclase and oxide crystals from 12 FLC samples are reported in Supplementary Data Table 4. Olivine crystals generally have low forsterite contents, from Fo (forsterite wt %) 72 to 56 (with the most common values around Fo_{64}), and each crystal is remarkably uniform in composition. NiO varies between 0·08 and ~~0·2~~ wt % and MnO between 0·2 and 0·6 wt %. The olivines are relatively evolved and never in equilibrium with their respective whole-rocks (given the olivine/melt K_D Fe/Mg = 0·30 ± 0·03; Roeder &

Emslie, 1970), in agreement with the cumulative nature of these rocks. Also, the markedly flat compositional profiles of olivine crystals may reflect Fe–Mg interdiffusion processes (Costa & Chakraborty, 2004; Chakraborty, 2010), which can plausibly affect olivine crystals when these are slowly and isobarically cooled in a large magma chamber. This makes olivine unsuitable for calculating the Mg# of the FLC parental magmas.

Plagioclase crystals vary from An (anorthite wt %) 73 to 56 (the vast majority being labradorites, with a few bytownites) and contain less than 3% orthoclase. Detailed core–rim traverses mostly show flat profiles, except for an inversely zoned plagioclase from sample SL12 (crystal rim reaches up to An_{83}) and other slight inverse zonings (An increasing from 55–58 to 61 towards the rim) in crystals from eight samples. Anorthite content is negatively correlated with K_2O concentration. Plagioclase crystals from sample SL18 show distinctly higher K_2O than the other samples (0·5–0·6 vs 0·2–0·4 wt %; $> Or_3$). The preservation of compositional zoning, however faint, and the anticorrelation between An and K_2O argue against complete diffusive re-equilibration of FLC plagioclase, which is a much slower process than Mg–Fe diffusion in olivine under the same conditions (Costa *et al.*, 2003).

Augite ($Wo_{20–45}En_{39–57}Fs_{11–31}$) crystals are nearly ubiquitous and in the investigated samples commonly have Mg# around 79 [calculated as atomic 100 × Mg/(Mg + Fe^{2+}); Fe^{2+} calculated from Fe_{tot} after Papike *et al.* (1974)]. Al_2O_3 varies from 1·32 to 3·31 wt % and is positively correlated with Mg#, as are TiO_2 (0·42–1·79 wt %) and Cr_2O_3 (<0·43 wt %). Many of the analysed augites have pigeonite exsolution ($Wo_{6–19}En_{51–69}Fs_{21–35}$, Mg# 76–62). Orthopyroxene ($Wo_{2–5}En_{58–72}Fs_{25–39}$, Mg# 65–70) is present in some of the analysed samples, often rimming olivine crystals. It frequently shows lamellae of exsolved clinopyroxene. Concentrations of TiO_2 in clinopyroxene from the FLC are systematically higher than those observed in clinopyroxene crystals from previously studied low-Ti CAMP rocks. Notably, only clinopyroxene from high-Ti CAMP rocks overlaps FLC clinopyroxene in terms of TiO_2 content (Fig. 6).

Oxides are present either enclosed within crystals or interstitially. Analyses of 12 samples revealed the presence of Ti-magnetite (TiO_2 up to 22 wt %; FeO_t up to 88 wt %) and ilmenite (TiO_2 up to 53 wt %; FeO_t up to 55 wt %). TiO_2 contents in Ti-magnetite crystals from SL18 are invariably low (<5 wt %). Oxides from the FLC show evidence of exsolution, with Ti-magnetite and ilmenite sub-solidus arrangements [previously observed also by Hargraves *et al.* (1999)].

WHOLE-ROCK GEOCHEMISTRY

Major element chemistry

The FLC intrusive samples all have subalkaline (Na_2O + K_2O from 0·76 to 4·31 wt %; Table 1) mafic compositions and generally low TiO_2 contents (0·07–1·44 wt %), with sample SL12 representing an exception at 2·00 wt % TiO_2.

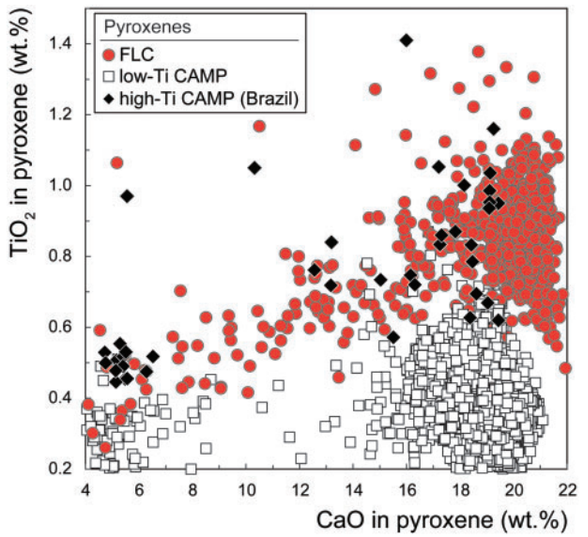

Fig. 6. Crystal chemistry (CaO and TiO_2, EMP analyses) of FLC pyroxenes compared with that of other pyroxenes from low- and high-Ti CAMP occurrences, showing that overlap exists only between FLC and high-Ti CAMP pyroxenes. Data for crystals from high-Ti rocks are from Cassiporè–Amapa dykes, Brazil (De Min *et al.*, 2003), and Maranhão Basin dykes and flows, Brazil (Merle *et al.*, 2011). Data from low-Ti CAMP pyroxenes are from Callegaro *et al.* (2013, 2014), Marzoli *et al.* (2014) and Merle *et al.* (2014).

The strong negative correlations between MgO (28·1–1·26 wt %) and SiO_2 (39·7–52·5 wt %), Al_2O_3 (5·63–27·2 wt %), CaO (2·77–14·7 wt %), and Na_2O (0·72–3·95 wt %), and the positive correlation of MgO with FeO_{tot} (22·5–2·82 wt %) indicate that rock compositions, as usually observed for cumulate rocks, are controlled by the relative proportions of the modal phases, in particular olivine, plagioclase, and clinopyroxene (Fig. 7). The dyke, closer to the composition of a basaltic liquid, is a clear outlier. It is a moderately evolved (Mg# 40) high-Ti (TiO_2 = 3·56 wt %) dolerite and has, at a comparable MgO content (5·23 wt %), lower SiO_2, Al_2O_3, CaO, and Na_2O and higher K_2O, Fe_2O_{3tot}, and P_2O_5 than the intrusive samples.

Maximum total loss on ignition is 0·5 wt %, suggesting only very minor alteration of the analysed samples. Our FLC samples fall within the compositional fields defined by previously published data from the FLC, including 63 intrusive rocks and three dykes (Fig. 7; Chalokwu, 2001). However, our dataset extends the compositional trends towards higher MgO contents (28·1 versus ~20 wt %).

Trace element chemistry

Trace element abundances were analysed on a subset (20 samples; Table 2 and Supplementary Data Table 5) of those samples for which major element concentrations were measured. Normalized to primitive mantle (PM; Sun & McDonough, 1989; Fig. 8a), the intrusive samples show a wide range of incompatible element (IE) concentrations, varying from more than 10 times

Table 1: Major element compositions (X-ray fluorescence) in wt % for FLC intrusive rocks and a cross-cutting doleritic dyke

	SiO_2	TiO_2	Al_2O_3	$Fe_2O_{3\,t}$	MnO	MgO	CaO	Na_2O	K_2O	P_2O_5	LOI	Total
Zone 1												
SL2	46·53	0·85	18·88	13·65	0·14	10·13	8·36	2·70	0·26	0·05	–0·79	100·87
SL1	46·01	0·83	18·22	14·05	0·14	10·33	7·87	2·61	0·26	0·05	–0·59	99·82
SL6	48·17	0·56	20·85	9·91	0·11	7·96	9·43	2·86	0·28	0·06	–0·39	99·89
SL7	49·34	1·16	15·84	12·92	0·18	9·21	9·58	2·17	0·11	0·01	–0·51	100·12
SL11	46·85	1·01	19·43	12·82	0·13	8·25	8·95	2·84	0·25	0·03	–0·53	100·05
SL12	43·18	2·00	15·30	18·89	0·18	10·50	8·12	2·19	0·18	0·02	–0·95	99·68
SL18	50·52	0·31	16·53	9·77	0·16	8·58	12·22	2·19	0·27	0·02	–0·15	100·49
SL20	51·74	0·65	20·52	6·07	0·10	5·16	13·15	2·97	0·22	0·01	0·03	100·69
SL21	45·65	0·85	18·46	14·74	0·14	10·66	7·96	2·63	0·22	0·02	–0·87	100·51
SL33	44·49	0·61	14·32	17·61	0·20	15·26	6·84	2·02	0·20	0·04	–0·95	100·7
SL34	45·44	0·65	15·56	15·88	0·18	13·54	7·41	2·20	0·23	0·05	–0·72	100·49
SL35	45·43	0·63	15·33	16·20	0·18	13·81	7·37	2·18	0·23	0·05	–0·81	100·68
Zone 2												
SL13	46·74	1·17	15·07	13·83	0·16	10·25	10·89	2·12	0·15	0·01	–0·48	99·97
SL14	51·05	0·83	18·98	7·32	0·11	5·86	13·16	2·67	0·19	0·02	–0·19	100·12
SL15	48·31	0·27	19·49	8·61	0·11	10·31	11·38	2·22	0·17	0·02	–0·36	100·58
SL17	50·92	0·51	18·29	6·37	0·11	7·67	14·34	2·20	0·14	0·02	0·05	100·67
Zone 3												
SL10	50·72	0·71	23·90	6·30	0·07	3·54	11·42	3·41	0·29	0·03	–0·09	100·38
SL41	48·04	0·38	17·80	11·66	0·14	10·38	9·80	2·48	0·20	0·02	–0·32	100·65
SL42	42·21	0·46	8·05	24·67	0·29	20·52	4·70	1·18	0·15	0·04	–1·49	100·82
SL43	49·06	1·44	19·95	10·26	0·12	5·42	10·66	2·97	0·30	0·05	0·02	100·33
SL44	46·46	0·38	17·37	13·82	0·16	12·50	7·94	2·41	0·21	0·03	–0·59	100·76
SL45	41·63	0·71	9·24	23·23	0·26	19·72	5·57	1·31	0·10	0·03	–1·41	100·46
Zone 4												
SL4	45·61	0·24	12·96	14·17	0·18	17·19	8·57	1·65	0·10	0·02	–0·57	100·21
SL22	47·3	0·38	11·42	13·96	0·20	15·59	10·64	1·52	0·09	0·02	–0·68	100·54
SL23	50·68	0·50	14·35	8·75	0·15	10·31	13·93	1·91	0·12	0·01	–0·07	100·73
SL26	52·48	0·59	27·15	3·14	0·04	1·26	11·71	3·95	0·36	0·02	0·08	100·88
SL28	39·67	0·07	5·63	24·97	0·30	28·10	2·77	0·72	0·04	0·02	–1·55	100·85
SL29	41·52	0·12	7·68	22·01	0·27	24·96	4·40	0·98	0·05	0·02	–1·36	100·73
SL30	45·96	0·22	13·49	13·75	0·18	16·69	8·90	1·71	0·10	0·01	–0·54	100·55
SL31	50·36	0·46	18·91	7·34	0·11	7·38	13·05	2·51	0·16	0·01	0·15	100·55
SL32	50·25	0·69	14·63	8·83	0·15	8·77	14·65	2·01	0·15	0·04	0·07	100·34
SL38	47·93	0·88	19·49	12·15	0·15	7·35	10·08	2·88	0·21	0·01	–0·35	100·86
Dyke												
SL39	47·52	3·56	11·97	18·24	0·25	5·23	9·33	2·45	0·80	0·34	0·51	100·35

PM to as low as 0·1 times PM. Their overall low IE contents are consistent with their cumulative character. They all have very similar compositional patterns with Ba, K, Pb, Sr, Eu, and Ti spikes and Nb troughs. Two samples stand out. Sample SL28 is markedly depleted, in agreement with its olivine-dominated mineralogy, whereas sample SL18N is the only sample with a negative Ti anomaly. Compared with the intrusive samples, the doleritic dyke (SL39) has higher concentrations of incompatible trace elements. It shares positive anomalies in Pb and Ti with the intrusive samples, but contrary to these has negative anomalies in Sr and K, possibly reflecting the removal of cumulate plagioclase or the effects of alteration. Also, the dyke has essentially no Nb anomaly.

In chondrite-normalized (McDonough & Sun, 1995; Fig. 8b) REE diagrams the intrusive samples show variable concentrations of REE (from 0·3 to 20 times chondritic abundances) and they all have a positive Eu anomaly ($Eu/Eu^* = 2·0–5·5$) reflecting plagioclase accumulation. The fractionation between light and heavy REE (LREE/HREE; La_{CH}/Yb_{CH} 1·6–8·1; subscript CH indicates chondrite-normalized values) correlates positively with LREE concentration. SL28 again is distinctly depleted, whereas SL18 displays the highest HREE concentrations. The dyke again stands out as an outlier, with markedly higher REE concentrations, typical of a basaltic liquid, and no Eu anomaly. The IE and REE patterns of the dyke (OIB-like, except for the lack of a Nb peak; Fig. 8) resemble those of other CAMP high-Ti basaltic rocks (Dupuy *et al.*, 1988; De Min *et al.*, 2003; Deckart *et al.*, 2005; Merle *et al.*, 2011).

ISOTOPES

Sr–Nd–Hf–Pb isotopes

The Sr–Nd–Hf–Pb isotopic compositions of the 19 intrusive FLC whole-rock samples and the doleritic dyke (the same sample subset as also analysed for trace element abundances) are reported as initial ratios at 200 Ma, using for age correction the trace element concentrations measured on different aliquots of the same sample powders (Tables 2 and 3). Most of the FLC samples define a tight cluster in Sr–Nd isotope space ($^{87}Sr/^{86}Sr_i$ = 0·703653–0·704019; $^{143}Nd/^{144}Nd_i$ = 0·512408–0·512510; $\varepsilon_{Ndi} = +0·5 – +2·5$; Fig. 9a). Samples SL28 and SL38 (both Zone 4) are moderate outliers. At

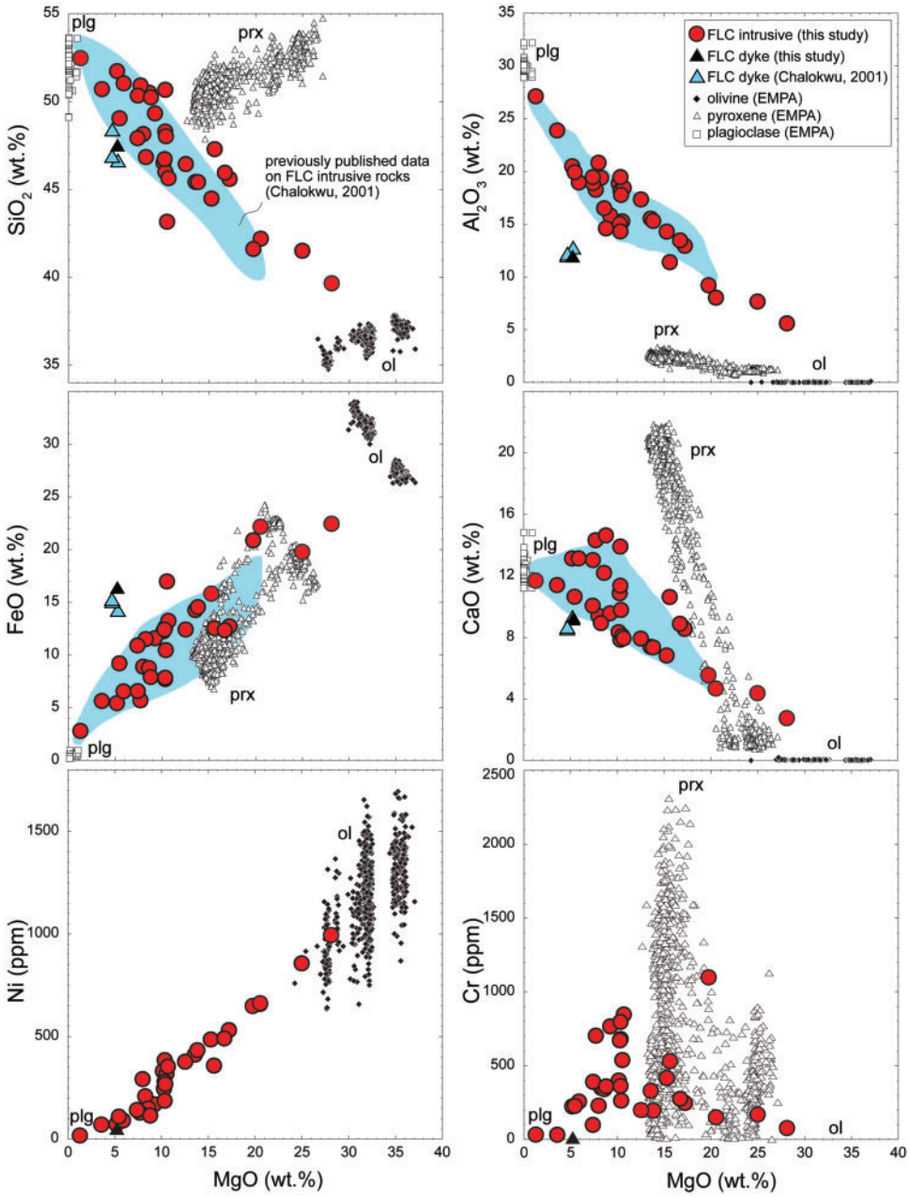

Fig. 7. Major and compatible trace element data (XRF; MgO vs SiO_2, Al_2O_3, FeO, CaO, in wt %; Ni and Cr, in ppm) for the FLC whole-rock samples (red circles for intrusive samples; black triangle for the dyke SL39) plotted along with EMP analytical points for their component minerals (olivine, plagioclase and pyroxenes). The compositions and modal proportions of the mineral phases (in particular, olivine, plagioclase and clinopyroxene) control the whole-rock compositions of the FLC samples. Whole-rock data points are enclosed within the ideal compositional polygons formed by the major constituent phases, a characteristic also visible for compatible trace elements such as Ni (19–996 ppm), Cr (34–1100 ppm), and Sc (5–40 ppm; not plotted). Nickel contents correlate positively with MgO, whereas Cr and Sc are enriched in rocks containing ~10 wt % MgO. Olivine control on Ni and clinopyroxene control on Cr are particularly visible. Plotted also are the compositions for intrusive rocks (blue field) and doleritic dykes (blue triangles) from Chalokwu (2001).

comparable $^{87}Sr/^{86}Sr_i$ (0·703760), SL28 plots at lower $^{143}Nd/^{144}Nd_i$ (0·512265; $\varepsilon_{Ndi} = -2{\cdot}3$). Conversely, SL38 has higher $^{143}Nd/^{144}Nd_i$ (0·512520; $\varepsilon_{Ndi} = +2{\cdot}7$) with respect to the cluster, coupled with lower $^{87}Sr/^{86}Sr_i$ (0·703378). Similarly, the dyke (SL39) plots at lower $^{87}Sr/^{86}Sr_i$ (0·703114) and higher $^{143}Nd/^{144}Nd_i$ (0·512590; $\varepsilon_{Ndi} = +4{\cdot}1$), towards the depleted MORB mantle (DMM) end-member (Zindler & Hart, 1986). Sample SL18N is an extreme outlier and plots at much higher $^{87}Sr/^{86}Sr_i$ (0·706506) and lower $^{143}Nd/^{144}Nd_i$ (0·511515; $\varepsilon_{Ndi} = -16{\cdot}9$). However, the gabbroic aliquot of this sample (SL18G; Fig. 3), devoid of poikilitic orthopyroxene, has a Sr–Nd isotopic composition within the range of the other samples (0·703960–0·512447; $\varepsilon_{Ndi} = +1{\cdot}3$).

Tab Incompatible trace element ~~compositions~~ (ICP-MS), including the rare earth elements, in ppm, for a subset of intrusive rocks from the FLC and the cross-cutting doleritic dyke

	Rb	Sr	Zr	Nb	Hf	Ta	Pb	Th	U	La	Ce	Pr	Nd	Sm	Eu	Gd	Tb	Dy	Ho	Er	Tm	Yb	Lu
Zone 1																							
SL02	1·09	345	10·51	1·92	0·85	0·46	0·77	0·16	0·03	1·38	3·24	0·41	1·55	0·35	0·42	0·33	0·06	0·26	0·07	0·17	0·03	0·15	0·04
SL06	3·05	380	20·55	2·23	0·61	0·28	1·67	0·33	0·08	3·90	9·21	1·17	4·36	0·99	0·92	0·95	0·18	0·82	0·21	0·50	0·11	0·40	0·09
SL12	1·04	275	11·27	1·00	0·37	0·13	0·87	0·09	0·02	1·51	3·61	0·48	2·08	0·56	0·60	0·67	0·12	0·62	0·15	0·39	0·06	0·31	0·05
SL18	1·45	351	10·02	0·30	0·35	0·06	1·41	0·06	0·01	2·67	6·24	0·86	3·71	1·05	0·76	1·28	0·25	1·37	0·34	0·92	0·14	0·72	0·12
SL34	2·84	279	22·69	1·76	0·56	0·13	1·28	0·28	0·06	3·08	7·50	0·98	3·67	0·89	0·72	0·91	0·16	0·84	0·20	0·53	0·08	0·42	0·08
Zone 2																							
SL13	0·57	270	7·61	0·34	0·33	0·08	0·82	0·03	0·01	1·11	3·00	0·49	2·26	0·78	0·67	0·99	0·19	1·03	0·26	0·63	0·09	0·47	0·08
SL15	0·90	336	5·76	0·31	0·21	0·10	0·85	0·04	0·01	1·56	3·64	0·49	2·13	0·57	0·68	0·66	0·13	0·62	0·15	0·38	0·06	0·29	0·05
SL17	1·01	330	11·55	0·47	0·43	0·08	0·84	0·06	0·02	1·83	4·86	0·74	3·45	1·13	0·81	1·33	0·26	1·36	0·31	0·80	0·12	0·57	0·10
Zone 3																							
SL10	2·01	474	10·61	1·03	0·34	0·21	1·24	0·16	0·04	2·53	5·91	0·78	2·94	0·71	1·01	0·71	0·12	0·62	0·14	0·36	0·06	0·27	0·05
SL42	2·02	170	18·33	2·70	0·53	0·19	0·95	0·26	0·05	2·73	6·63	0·87	3·42	0·82	0·62	0·90	0·17	0·89	0·22	0·61	0·10	0·53	0·10
SL43	3·09	371	33·08	2·85	0·92	0·22	1·25	0·30	0·08	3·95	9·88	1·31	5·40	1·36	1·08	1·49	0·28	1·42	0·34	0·89	0·13	0·64	0·11
SL44	1·52	301	10·72	0·90	0·26	0·09	0·88	0·14	0·03	1·91	4·43	0·58	2·10	0·47	0·61	0·46	0·08	0·40	0·10	0·26	0·04	0·21	0·04
SL45	0·51	158	5·26	0·43	0·16	0·05	0·48	0·03	0·01	0·82	2·00	0·28	1·21	0·37	0·38	0·41	0·08	0·41	0·11	0·29	0·04	0·25	0·05
Zone 4																							
SL4	0·54	237	5·05	0·25	0·18	0·06	0·48	0·03	0·01	1·04	2·64	0·37	1·64	0·50	0·48	0·60	0·11	0·60	0·14	0·37	0·05	0·29	0·05
SL26	2·57	495	11·94	2·57	0·35	0·20	1·24	0·09	0·02	3·01	6·76	0·83	3·10	0·67	1·18	0·64	0·11	0·56	0·13	0·34	0·05	0·25	0·04
SL28	0·29	98	1·27	0·08	0·03	0·01	0·39	0·01	0·01	0·43	0·93	0·10	0·41	0·09	0·12	0·07	0·02	0·08	0·02	0·08	0·01	0·08	0·02
SL29	0·42	130	6·15	0·18	0·17	0·03	0·38	0·04	0·01	0·68	1·66	0·23	0·99	0·26	0·19	0·30	0·06	0·29	0·07	0·19	0·03	0·18	0·03
SL30	0·37	241	4·09	0·16	0·15	0·04	0·45	0·01	0·00	0·81	2·06	0·30	1·47	0·47	0·45	0·56	0·11	0·56	0·14	0·37	0·05	0·26	0·05
SL38	0·92	443	7·11	0·98	0·23	0·08	0·72	0·03	0·01	1·96	4·30	0·56	2·12	0·54	0·90	0·59	0·11	0·56	0·13	0·35	0·05	0·29	0·05
Dyke																							
SL39	22·70	309	209·5	·68	5·73	1·75	4·31	2·98	0·95	30·95	65·17	9·84	38·05	8·44	2·96	8·56	1·51	7·48	1·76	4·64	0·65	3·33	0·54

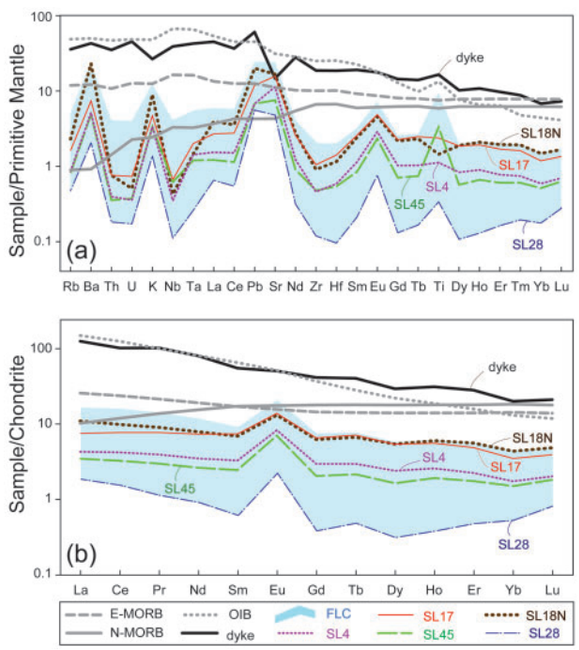

Fig. 8. Incompatible (a) and rare earth element (b) compositions for whole-rocks from the FLC samples plotted in multi-element diagrams and normalized, respectively, to the Primitive Mantle (Sun & McDonough, 1989) and C1 chondrites (McDonough & Sun, 1995). The shaded field represents the total range of compositions covered by the sample set, and the individual patterns of the dyke and the intrusive samples SL4, SL17, SL28, SL18N and SL45 are highlighted. For comparison, OIB, normal (N)-MORB and enriched (E)-MORB patterns also are plotted (data source: Sun & McDonough, 1989).

The relatively unradiogenic $^{87}Sr/^{86}Sr_i$ of the main cluster of samples is consistent with the initial value of 0·70389 reported for a whole-rock Rb–Sr isochron by Beckinsale *et al.* (1977). All the samples (except SL18N) plot within the isotopic space defined by the DMM, EMI, and EMII mantle end-members (Zindler & Hart, 1986).

We present here the first Hf isotopic data obtained for CAMP rocks. The FLC samples cluster within a restricted $^{176}Hf/^{177}Hf_i$ range (0·282790–0·282864, $\varepsilon_{Hfi} = +5{\cdot}0 - +7{\cdot}3$; Table 3; Fig. 9b), which is positively correlated with $^{143}Nd/^{144}Nd_i$, overlapping the OIB and MORB fields on the terrestrial array (Blichert-Toft & Albarède, 1997; Vervoort *et al.*, 1999; Jourdan *et al.*, 2007). The dyke has more radiogenic Hf (0·282904; $\varepsilon_{Hfi} = +9{\cdot}1$), and is thus displaced towards the depleted mantle isotopic field. Samples SL28 and SL4 are moderate outliers—SL28 plots below the Hf–Nd alignment, at lower $^{176}Hf/^{177}Hf_i$ (0·282634; $\varepsilon Hf_i = -0{\cdot}5$), whereas SL4 plots above the Hf–Nd alignment to the left of the main cluster ($^{176}Hf/^{177}Hf_i = 0{\cdot}282818$; $\varepsilon Hf_i = +6{\cdot}0$). SL18N, with very low $^{176}Hf/^{177}Hf_i$ (0·282056; $\varepsilon Hf_i = -20{\cdot}9$), remains an extreme outlier, not only with respect to the other FLC samples, but also when compared with oceanic basalts worldwide; that is, it falls on the less radiogenic end of the field defined by sediments (upper crust; Vervoort *et al.*, 1999; Chauvel *et al.*, 2008). Hafnium isotopic compositions were also measured on the baddeleyites separated from SL18G for U–Pb geochronology. The marked Sr and Nd isotopic differences between the two rock portions of SL18 (Fig. 3) is likewise observed for Hf isotopes; whereas SL18N has unradiogenic $^{176}Hf/^{177}Hf$, baddeleyites from SL18G share the same Hf isotopic composition as the majority of the FLC samples, ranging from 0·282807 ± 0·000016

AQ19 **Table 3:** Measured and initial (200 Ma) isotopic ratios for a subset of intrusive rocks from the FLC and the cross-cutting doleritic dyke

Sample	$^{87}Sr/^{86}Sr$	2σ	$^{87}Sr/^{86}Sr_i$	2σ	$^{176}Hf/^{177}Hf$	2σ	ε_{Hf}	$^{176}Hf/^{177}Hf_i$	ε_{Hfi}	$^{143}Nd/^{144}Nd$	2σ	ε_{Nd}	$^{143}Nd/^{144}Nd_i$	ε_{Ndi}	$^{206}Pb/^{204}Pb$	$^{207}Pb/^{204}Pb$	$^{208}Pb/^{204}Pb$	$^{206}Pb/^{204}Pb_i$	$^{207}Pb/^{204}Pb_i$	$^{208}Pb/^{204}Pb_i$
Zone 1																				
SL02	0·703966	19	0·703940	22	0·282876	5	3·68	0·282853	7·26	0·512597	15	−0·80	0·512417	0·70	17·664	15·593	37·917	17·353	15·578	37·545
SL06	0·704010	15	0·703944	22	0·282888	6	4·10	0·282807	5·61	0·512593	17	−0·88	0·512413	0·63	17·673	15·588	37·923	17·350	15·572	37·585
SL12	0·703928	27	0·703897	30	0·282900	8	4·53	0·282825	6·26	0·512622	13	−0·31	0·512409	0·54	17·660	15·587	37·913	17·389	15·574	37·582
SL18N	0·706540	19	0·706506	22	0·282240	7	−18·81	0·282056	−20·93	0·511740	7	−17·52	0·511516	−16·89	16·628	15·612	36·973	16·399	15·601	36·624
SL18G	0·703993		0·703960							0·512672		0·66	0·512447	1·30	—	—	—	—	—	
SL34	0·703996	14	0·703912	22	0·282880	4	3·82	0·282809	5·69	0·512633	12	−0·10	0·512442	1·18	17·710	15·592	37·965	17·579	15·585	37·786
Zone 2																				
SL13	0·703780	31	0·703763	33	0·282925	9	5·41	0·282794	5·16	0·512711	8	1·42	0·512440	1·15	17·654	15·595	37·920	17·579	15·591	37·759
SL15	0·703902	14	0·703880	16	0·282924	28	5·38	0·282800	5·37	0·512662	8	0·47	0·512452	1·39	17·546	15·584	37·779	17·366	15·575	37·389
SL17	0·703882	25	0·703857	28	0·282938	7	5·87	0·282816	5·94	0·512740	8	1·99	0·512482	1·97	17·886	15·590	37·985	17·768	15·584	37·757
Zone 3																				
SL10	0·704054	12	0·704019	15	0·282902	7	4·60	0·282826	6·30	0·512636	22	−0·04	0·512445	1·24	17·652	15·571	37·846	17·327	15·554	37·454
SL42	0·703941	16	0·703843	26	0·282920	5	5·23	0·282824	6·22	0·512663	3	0·49	0·512473	1·79	17·693	15·578	37·916	17·541	15·571	37·684
SL43	0·703968	18	0·703899	25	0·282888	5	4·10	0·282826	6·30	0·512660	14	0·43	0·512462	1·57	17·672	15·582	37·907	17·549	15·576	37·688
SL44	0·703948	19	0·703906	23	0·282884	17	3·96	0·282810	5·73	0·512639	19	0·02	0·512464	1·61	17·695	15·593	37·925	17·586	15·587	37·784
SL45	0·703930	15	0·703903	18	0·282937	12	5·84	0·282790	5·01	0·512664	7	0·51	0·512424	0·83	17·551	15·581	37·769	17·462	15·577	37·594
Zone 4																				
SL04	0·703779	22	0·703760	24	0·282970	17	7·00	0·282818	6·02	0·512505	22	−2·60	0·512266	−2·26	17·614	15·559	37·787	17·488	15·553	37·531
SL26	0·703875	15	0·703832	19	0·282894	6	4·31	0·282830	6·46	0·512681	21	0·84	0·512511	2·53	17·617	15·551	37·780	17·454	15·543	37·455
SL28	0·703722	14	0·703698	16	0·283004	52	8·20	0·282634	−0·50	0·512625	9	−0·25	0·512453	1·39	17·771	15·570	37·886	17·646	15·563	37·723
SL29	0·703680	33	0·703653	36	0·282946	18	6·15	0·282849	7·10	0·512702	6	1·25	0·512497	2·26	17·697	15·573	37·901	17·437	15·560	37·606
SL30	0·703774	23	0·703761	24	0·282979	20	7·32	0·282805	5·57	0·512679	16	0·80	0·512427	0·88	17·819	15·586	37·938	17·749	15·582	37·792
SL38	0·703391	17	0·703374	19	0·282981	15	7·39	0·282864	7·66	0·512720	11	1·60	0·512521	2·73	17·725	15·528	37·713	17·565	15·520	37·362
Dyke																				
SL39	0·703718	26	0·703111	87	0·282954	4	6·44	0·282904	9·07	0·512766	6	2·50	0·512591	4·10	18·138	15·563	38·096	18·088	15·560	38·003

Sample SL18 is split into SL18G and SL18N, representing, respectively, the gabbroic and noritic parts. Details on the analytical methods and the uncertainties of measured and initial isotopic compositions are given in the Supplementary Data. The reported 2σ errors refer to the last decimal places.

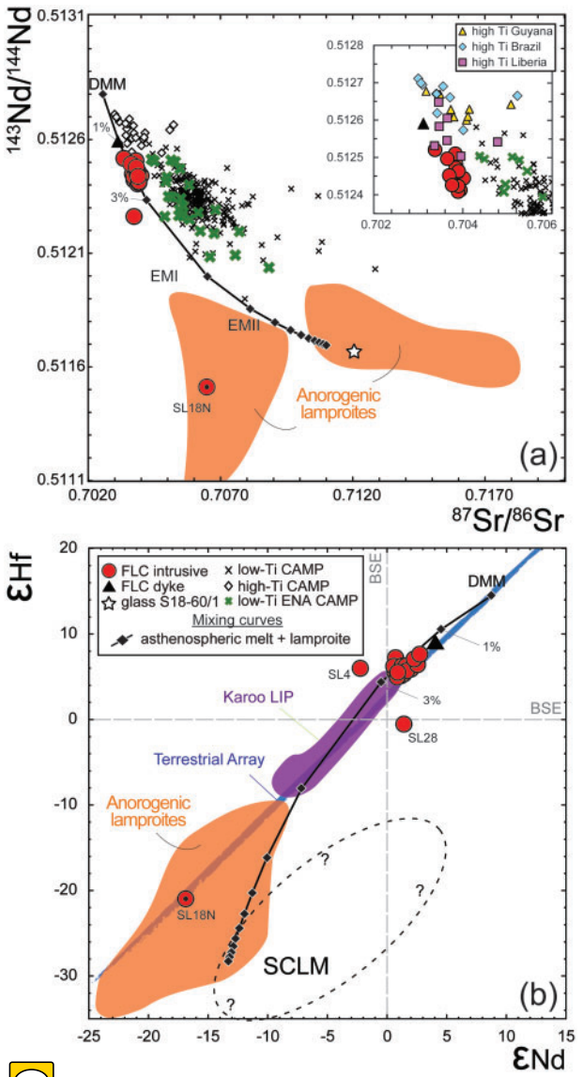

Fig. 9. (a) Initial (200 Ma) Sr–Nd isotopic compositions for the FLC rocks. Black continuous line is mixing curve between asthenospheric and lamproitic melts. Black diamonds mark 1%, 3% (indicated) and 10% steps of mixing. Compositions of the lamproitic and asthenospheric melts are given in Table 5. Low-Ti and high-Ti CAMP data (whole-rock) are taken from Callegaro *et al.* (2014), Merle *et al.* (2014) and references therein. Isotopic fields for lamproites are reported as present-day values and are as given by Bergman (1987) and Mirnejad & Bell (2006). The EMI, EMII and DMM mantle end-members are reported back-corrected to 200 Ma. The composition of the andesitic glass S18-60/1 from Kamenetsky *et al.* (2001) also is shown (white star). The inset shows the main data cluster from the FLC (large dots) plotted along with other high-Ti CAMP rocks listed in the legend according to their geographical provenance (triangles for Guyana, diamonds for Brazil and squares for Liberia). (b) ε_{Nd}–ε_{Hf} diagram (isotopic values back-corrected to 200 Ma). The terrestrial array follows the relationship $\varepsilon_{Hf} = 1{\cdot}5\varepsilon_{Nd} + 1{\cdot}28$ (Jourdan *et al.*, 2007). Fields for SCLM and anorogenic lamproites are as given by Griffin *et al.* (2000); field for the Karoo LIP as given by Jourdan *et al.* (2007). ε_{Hf} is calculated with a 200 Ma CHUR value for $^{176}Hf/^{177}Hf_i$ of 0·282648, from present-day values of 0·282772 and 0·0332 for $^{176}Hf/^{177}Hf$ and $^{176}Lu/^{177}Hf$, respectively, following Blichert-Toft & Albarède (1997); ε_{Nd} calculated following Jacobsen & Wasserburg (1980). Here and in the following figures sample SL18N is highlighted with a bull's eye symbol.

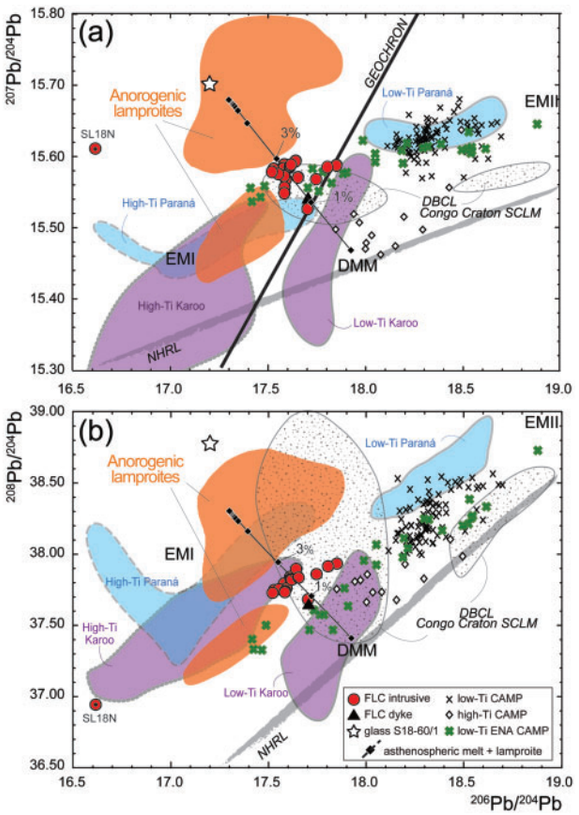

Fig. 10. Initial (200 Ma) Pb isotopic compositions for the FLC. Mixing lines as in Fig. 9. The northern hemisphere reference line (NHRL) is reported for present-day values. The DMM, EMI and EMII reservoirs are back-corrected to 200 Ma. The field for the Congo Craton SCLM and Damaraland ultra-alkaline rocks (DBCL) is from Le Roex & Lanyon (1998). The composition of the andesitic glass S18-60/1 from Kamenetsky *et al.* (2001) is also shown (white star). Previously published isotopic data from low-Ti and high-Ti CAMP (Callegaro *et al.*, 2014; Merle *et al.*, 2014; and references therein), Paraná–Etendeka and Karoo LIPs are from Peate *et al.* (1999), Rocha-Júnior *et al.* (2013) and Jourdan *et al.* (2007), respectively.

to 0·282820 ± 0·000015 and corresponding to εHf_i values of +5·6 – +6·1 (Supplementary Data Table 3).

Most of the FLC samples have uniform Pb isotopic compositions ($^{206}Pb/^{204}Pb_i$ = 17·520–17·850, $^{207}Pb/^{204}Pb_i$ = 15·549–15·594 and $^{208}Pb/^{204}Pb_i$ = 37·730–37·936; Fig. 10) with the rare feature of clustering to the left of the Geochron in $^{207}Pb/^{204}Pb_i$–$^{206}Pb/^{204}Pb_i$ space. The FLC samples plot above the Northern Hemisphere Reference Line (NHRL; Hart, 1984), roughly between the EMI and EMII end-members (Hofmann, 2003), having markedly high Δ7/4 {15·2–19·2; calculated as 100 × [$^{207}Pb/^{204}Pb_i$ – ($^{206}Pb/^{204}Pb_i$ × 0·1084 + 13·491)]}. The dyke and sample SL38, similar to what is observed for Sr, Nd and Hf isotopes, are slightly separated from the cluster and plot towards the DMM field; that is, along the Geochron, at slightly lower Δ7/4 (11·6–13·1). In $^{208}Pb/^{204}Pb_i$–$^{206}Pb/^{204}Pb_i$ space, the FLC samples plot within the isotopic range of the DUPAL anomaly (Hart, 1984), but below the line connecting EMI and EMII.

Notably, these are the only sampled CAMP rocks to yield such high Δ8/4 {61·7–94·4; calculated as 100 × [$^{208}Pb/^{204}Pb_i$ – ($^{206}Pb/^{204}Pb_i$ × 1·209 + 15·627)]}. Sample SL18N again is an extreme outlier, with the lowest $^{206}Pb/^{204}Pb_i$ (16·614) and $^{208}Pb/^{204}Pb_i$ (36·945), and highest $^{207}Pb/^{204}Pb_i$ (15·611); that is, it falls at very high Δ7/4 (31·9) and Δ8/4 (123·2) with respect to the main sample cluster, in a region of Pb ~~isotopic~~ space approached only by some ancient (Archean) lower crustal reservoirs (compare Lashaine Archean granulitic xenoliths from Tanzania; Cohen *et al.*, 1984; North China Craton granulites; Ying *et al.*, 2010).

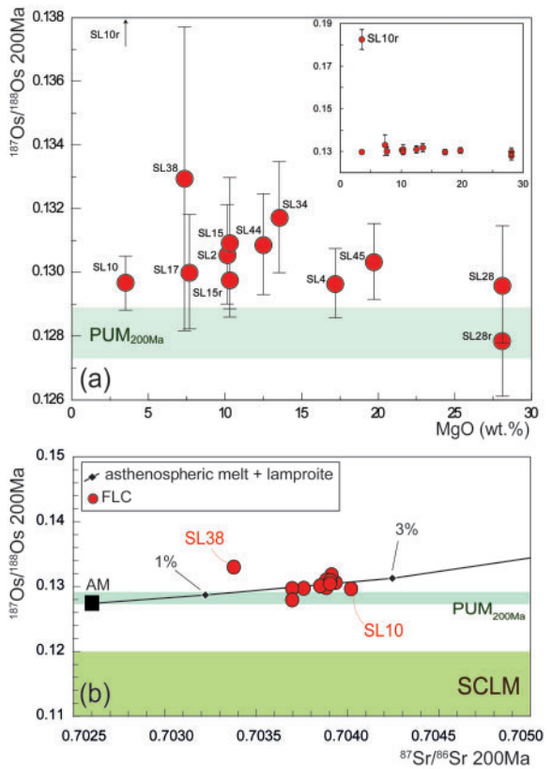

Fig. 11. (a) $^{187}Os/^{188}Os$ ~~isotopic ratios~~ for the FLC (back-calculated to 200 Ma) plotted as a function of MgO (wt %). Error bars for FLC samples include total uncertainty. Sample SL10r is shown in the inset only. (b) Mixing line as described in Fig. 9. Fields and ranges for PUM (back-calculated to 200 Ma) and SCLM as given by Shirey & Walker (1998) and Meisel *et al.* (2001).

Os isotopes

~~Of the FLC samples, 10~~ were selected for Re–Os isotopic analysis (a total of 13 analyses, including three replicates; Fig. 11; Table 4). Measured Os concentrations range from 0·27 to 1·17 ppb (mean = 0·815 ppb), with the exception of one aliquot of sample SL10 with a concentration as low as 0·068 ppb. Rhenium concentrations vary between 0·005 and 0·202 ppb. Consistent with their cumulate origin, Os concentrations in the FLC rocks are high compared with those of common basaltic rocks (generally <0·5 ppb Os; Shirey & Walker, 1998) and previously analysed CAMP basalts with comparable initial $^{187}Os/^{188}Os$ compositions (0·026–1·098 ppb; mean = 0·348 ppb; Merle *et al.*, 2011, 2014), although some overlap exists with CAMP dykes from Eastern North America (0·13–1·09 ppb; Callegaro *et al.*, 2013). Replicate analyses of sample SL28 agree well for both Re and Os concentrations and $^{187}Os/^{188}Os_i$, whereas replicates of SL15 agree less well for concentrations, but still yield ~~concordant~~ $^{187}Os/^{188}Os_i$ ratios. In contrast, replicates of sample SL10 show marked differences for both Re and Os concentrations and initial Os isotopic ratios, probably owing to a nugget effect, as discussed below.

Measured $^{187}Os/^{188}Os$ ranges between 0·12815 (SL28) and 0·13645 (SL38), again with the exception of aliquot SL10r (0·18474). Excluding this sample from a plot of $^{187}Os/^{188}Os$ as a function of $^{187}Re/^{188}Os$ yields an errorchron with an apparent age of 292 ± 120 Ma

Table 4: Measured and initial (200 Ma) Re–Os ~~isotopic ratios~~ and ~~trace element~~ abundances (ppb) for 10 FLC samples

Sample	[Os] (ppb)	[Re] (ppb)	$^{187}Re/^{188}Os$	$^{187}Os/^{188}Os$	In-run uncertainty (2σ)	$^{187}Os/^{188}Os$ initial	Total uncertainty (2σ)
Zone 1							
SL2	0·889	0·202	1·095	0·13423	0·00034	0·1306	0·0017
SL34	1·015	0·005	0·023	0·13182	0·00035	0·1317	0·0019
Zone 2							
SL15	0·835	0·027	0·156	0·13144	0·00035	0·1309	0·0022
SL15r	1·171	0·014	0·058	0·12998	0·00009	0·1298	0·0013
SL17	0·741	0·016	0·107	0·13039	0·00007	0·1300	0·0019
Zone 3							
SL10	2·080	0·228	0·528	0·13140	0·00015	0·1296	0·0010
SL10r	0·068	0·010	0·680	0·18474	0·00054	0·1825	0·0046
SL44	0·853	0·044	0·250	0·13173	0·00012	0·1309	0·0017
SL45	1·170	0·098	0·406	0·13170	0·00019	0·1304	0·0013
Zone 4							
SL4	0·548	0·017	0·153	0·13018	0·00021	0·1297	0·0013
SL28	0·736	0·012	0·075	0·12988	0·00011	0·1296	0·0019
SL28r	0·732	0·013	0·082	0·12815	0·00019	0·1279	0·0019
SL38	0·270	0·059	1·049	0·13645	0·00026	0·1329	0·0048

Analytical details are given in the Supplementary Data. Total uncertainties on initial $^{187}Os/^{188}Os$ ratios are 2σ and include in-run uncertainties, standard reproducibility, and the effects of Re blank variability on the $^{187}Re/^{188}Os$ ratios used for radiogenic ingrowth corrections.

(MSWD = 2·9) and an initial $^{187}Os/^{188}Os$ of 0·1298 ± 0·0010. The large uncertainty on this apparent age is due mainly to the small range of $^{187}Re/^{188}Os$ values (0·023–1·11), and to a lesser extent to minor initial isotopic heterogeneity and/or limited crustal contamination. With the exception of sample SL10r, the FLC rocks display a narrow compositional range in $^{187}Os/^{188}Os_i$ (0·1279 ± 0·0019 to 0·1329 ± 0·0048; 2σ, including all identified sources of uncertainty), which brackets the proposed Primitive Upper Mantle (PUM) value at 200 Ma (0·1281 ± 0·0008, calculated from the present-day value of PUM of 0·1296; Meisel *et al.*, 2001). $^{187}Os/^{188}Os_i$ does not show a clear correlation with Os concentration or MgO (Fig. 11). Nevertheless, sample SL10r, with the lowest Os concentration (0·068 ppb), also has the highest initial $^{187}Os/^{188}Os$ (0·1825 ± 0·0046), and sample SL38, likewise with a relatively low Os content (0·270 ppb), shows a slightly elevated initial $^{187}Os/^{188}Os$ (0·1329 ± 0·0048). No correlations exist between $^{187}Os/^{188}Os_i$ and the other measured isotopic ratios, although the radiogenic sample SL10r also has the most radiogenic $^{87}Sr/^{86}Sr_i$ (0·704019) with the exception of the unusual sample SL18N.

Our results can be compared with those obtained by Hattori *et al.* (1991) on eluvial platinum group element (PGE) nuggets found in the regolith above the FLC (exclusively above Zone 3). Hattori *et al.* (1991) provided strong evidence for a magmatic origin of both erlichmanite (OsS_2) nuggets and Pt–Fe alloys. The former have low $^{187}Os/^{188}Os_i$ (0·130–0·132), comparable with our whole-rock data, and have been interpreted by Hattori *et al.* (1991) as early magmatic crystallization products that escaped crustal contamination. Conversely, Pt–Fe alloys, which probably formed late in the crystallization history of the FLC, range in $^{187}Os/^{188}Os_i$ between 0·144 and 0·253, reflecting some interaction with crustal Os.

DISCUSSION

The age of the FLC

As is the case for most other basaltic provinces, the CAMP has been dated mainly by $^{40}Ar/^{39}Ar$ geochronology (e.g. Marzoli *et al.*, 2011), with only a few available U–Pb ages (Dunning & Hodych, 1990; Schoene *et al.*, 2010; Blackburn *et al.*, 2013; Davies *et al.*, 2017). The $^{40}Ar/^{39}Ar$ plateau ages (201·7 ± 0·8 and 202·4 ± 2·3 Ma) and the $^{206}Pb/^{238}U$ age (198·777 ± 0·22 Ma—uncertainty includes the tracer calibration and decay constant uncertainties so that the $^{40}Ar/^{39}Ar$ and U–Pb ages can be compared; see above) obtained here for three samples from the FLC all fall within the age density distribution curve for CAMP magmatism (Marzoli *et al.*, 2011; Davies *et al.*, 2017; Fig. 5). The dated samples, whose $^{40}Ar/^{39}Ar$ ages are indistinguishable within the uncertainties, come from Zone 1 (SL2) and Zone 4 (SL4); that is, from stratigraphically low and high portions of the complex, respectively. This would suggest rapid emplacement of the FLC, implying that even if multiple pulses were injected, these were not separated by time spans long enough to be resolved with the precision of the $^{40}Ar/^{39}Ar$ method. In contrast, the U–Pb age, which comes from a Zone 1 sample (SL18G), does not overlap with the $^{40}Ar/^{39}Ar$ ages but is significantly younger. This younger age could be biased by baddeleyite Pb loss, although all the single crystal analyses are concordant (Supplementary Data Table 3). If all of the baddeleyite crystals have experienced Pb loss, the $^{207}Pb/^{206}Pb$ age may provide the best estimate of the crystallization age. The weighted mean $^{207}Pb/^{206}Pb$ age for all the crystals is 201·19 ± 0·69/0·81/4·4 Ma, with an MSWD of 2·2, which overlaps the $^{40}Ar/^{39}Ar$ plagioclase age. However, because all the analyses are concordant and for the most part overlapping in age, it seems unlikely that seven of the 11 analyses should display exactly the same amount of Pb loss and move along the concordia to randomly produce an age with a 0·2 ‰ uncertainty (Supplementary Data Fig. 2). One baddeleyite analysis produced a slightly older age of 199·37 ± 0·36 Ma. This grain, which was interpreted as an antecryst, could be a better estimate of the baddeleyite crystallization age with all younger grains reflecting some degree of Pb loss. However, the oldest baddeleyite age still does not overlap with the $^{40}Ar/^{39}Ar$ age. Systematic differences between $^{40}Ar/^{39}Ar$ and $^{206}Pb/^{238}U$ ages for the same samples were common before the updated ^{40}K decay constant of Renne *et al.* (2010, 2011), but are no longer accepted as age differences now are less than 5‰ between the two techniques (Smith *et al.*, 2010; Meyers *et al.*, 2012; Renne *et al.*, 2013).

The $^{40}Ar/^{39}Ar$ age of SL4 shows signs of inherited ^{40}Ar owing to the upwards-convex nature of the plateau at higher temperatures. Inherited ^{40}Ar produces older ages and this age should therefore be considered a maximum age for that sample. However, the age spectrum of SL2 is of good quality, with homogeneous $^{40}Ar^*$ distribution in the sample, and lacking any sign of inherited ^{40}Ar. Therefore, this age is likely to genuinely represent the age of this portion of the intrusion at ~202 Ma.

Because both the $^{40}Ar/^{39}Ar$ and $^{206}Pb/^{238}U$ ages seem robust, we cannot exclude the possibility that SL2 represents an early intrusion, whereas SL18G represents a *c.* 3 Myr later injection from a similar source, even if textural evidence such as internal chilled zones or changes in grain size was not visible in the studied outcrop. A long emplacement history is also supported by the presence of samples with both normal and reverse polarity as determined by paleomagnetic studies of the FLC carried out by Briden (1977) and Hargraves *et al.* (1999). Likewise consistent with this theory is the observation of two chemical populations of apatite in sample SL18G, which may indicate a main magmatic pulse for the emplacement of the FLC (concordant with the main peak of CAMP activity), followed by a second magmatic pulse crystallizing baddeleyite. The apatite geochemistry suggests that a marked chemical change in apatite composition occurred between 198 and 200 Ma. Apatites with ages before and after this time are

remarkably homogeneous in composition (La/Yb 12·4–17·9; Supplementary Data Figs 3–4). We interpret the apatites with high La/Yb (19·0–32·4), crystallizing at ~199 Ma, to reflect crystallization from a late-stage melt, possibly related to fresh magma influx. The timing of change in magma composition corresponds well to the crystallization age of baddeleyite (198·777 ± 0·047/0·07/0·22 Ma) and possibly suggests that the young baddeleyite ages reflect late magma injection. The oldest apatite U–Pb age (205·4 ± 1·5 Ma) overlaps, within the uncertainties, with the $^{40}Ar/^{39}Ar$ date of 202·4 ± 2·3 Ma. The apatite in question is characterized by La/Yb of 15·8 and Th/U of 5·11. Previous studies (Cochrane *et al.*, 2014) have used variations in Th/U as an indicator of xenocrystic apatites or apatites with variable diffusion properties. However, the apatites considered here are characterized by a narrow range in Th/U, indicating that xenocrystic apatite is absent. The apatite ages that are younger than 198 Ma can be explained by excess Pb loss through volume diffusion as the Sierra Leone intrusion cooled slowly.

We note that the Palisades sill (North American CAMP) also yields $^{40}Ar/^{39}Ar$ ages ranging from 195·1 ± 2·1 Ma to 202·8 ± 1·8 Ma (Marzoli *et al.*, 2011). A relatively long intrusive history for the Palisades sill likewise is provided by zircon U–Pb ages, considering that the sill was formed from Orange Mt and Preakness basalt magmas (201·52 ± 0·03 and 201·27 ± 0·03 Ma, respectively; Blackburn *et al.*, 2013; compare Puffer *et al.*, 2009). Incrementally assembled plutons have been observed in felsic systems; for example, the Tuolumne intrusive suite in California assembled over ~10 Myr (Coleman *et al.*, 2009), whereas in mafic systems, geochronological results have tended to reveal rapid emplacement; for example, the Skaergaard intrusion assembled over ~600 kyr (Wotzlaw *et al.*, 2012) and the Bushveld intrusion assembled over ~1 Myr (Zeh *et al.*, 2015). Despite the geochronological complexity, all ages indicate that the FLC magmatism is part of the CAMP [as previously posited by Hattori *et al.* (1991)], but additional dating of other samples throughout the complex is needed to ascertain whether it was assembled incrementally and to further constrain (and explain) the observed age dispersion.

The FLC compared with other CAMP rocks

Whereas the FLC whole-rock samples, being mafic cumulates, unsurprisingly have low TiO_2 concentrations, their clinopyroxenes are Ti-rich (0·5–1·4 TiO_2 wt %; Fig. 6). Using a Ti $^{cpx/melt}K_D$ of *c.* 0·3 (e.g. Bédard, 2014) for basaltic melts at upper crustal pressures (<5 kbar; Chalokwu, 2001), we calculated that the FLC clinopyroxenes crystallized from a basaltic magma with ~1·5–3·3 wt % TiO_2, which means that the Freetown intrusion was fed by high-Ti magmas. The isotopic data for the FLC samples can be compared with those previously published for high-Ti (Dupuy *et al.*, 1988; De Min *et al.*, 2003; Deckart *et al.*, 2005; Merle *et al.*, 2011) and low-Ti (De Min *et al.*, 2003; Deckart *et al.*, 2005; Verati *et al.*, 2005; Callegaro *et al.*, 2013, 2014; Marzoli *et al.*, 2014; Merle *et al.*, 2014) CAMP rocks. Because of their more sporadic occurrence, fewer geochemical studies are available ~~of high-Ti CAMP rocks than of the low-Ti CAMP rocks~~, Whereas Sr and Nd isotopic data are available for most of the high-Ti CAMP occurrences in South America and Western Africa, Pb isotope compositions have so far been measured ~~on~~ only a few samples from Brazil and Guyana (Deckart *et al.*, 2005; Merle *et al.*, 2011), Os isotopes on only four samples from Brazil (Merle *et al.*, 2011), and Hf isotopes not at all.

In Sr–Nd isotope space (Fig. 9) the FLC plots at comparable $^{87}Sr/^{86}Sr_i$ but slightly lower $^{143}Nd/^{144}Nd_i$ than the other high-Ti CAMP rocks, overlapping only with some samples from Liberia (Dupuy *et al.*, 1988). The difference between the FLC and the low-Ti CAMP rocks is more pronounced, the latter generally showing more radiogenic Sr and less radiogenic Nd. The FLC also displays lower $^{206}Pb/^{204}Pb_i$ and higher Δ7/4 and Δ8/4 (Fig. 10) than almost all (both high- and low-Ti) previously studied CAMP rocks, the only exception being some low-Ti doleritic dykes from the southeastern USA (Callegaro *et al.*, 2013). These, however, are very different in terms of Sr–Nd isotope compositions, having higher $^{87}Sr/^{86}Sr_i$ and lower $^{143}Nd/^{144}Nd_i$. They also have slightly lower Δ8/4 at a given $^{206}Pb/^{204}Pb_i$ with respect to the FLC. The southeastern USA CAMP rocks also cover a larger range of Sr–Nd–Pb isotopic compositions compared with the homogeneous signature of the FLC (Figs 9–11), although this is not surprising given the much wider geographical dispersion of these tholeiites ~~with respect~~ to the restricted distribution of the FLC samples. Thus, despite some overlap in $^{207}Pb/^{204}Pb$–$^{206}Pb/^{204}Pb$ space, the different $^{208}Pb/^{204}Pb$ and Sr and Nd isotopic compositions, as well as the greater isotopic variability of the southeastern USA dykes, plus their low-Ti nature, distinguish them from the high-Ti rocks of the FLC and suggest that they do not share a common origin (see Callegaro *et al.*, 2013; Whalen *et al.*, 2015).

With the exception of one analysis from the highly differentiated sample SL10, Os isotope data for the FLC overlap the general, rather homogeneous, CAMP Os isotopic field. In particular, $^{187}Os/^{188}Os_i$ signatures for the FLC are similar to those obtained from previously analysed low-Ti CAMP basalts (from Eastern North America 0·1278–0·1442, SW Europe 0·123–0·138, and Brazil 0·1267–0·1299; Merle *et al.*, 2011, 2014; Callegaro *et al.*, 2013, 2014; Fig. 11). Of the four Os isotope measurements available for high-Ti CAMP rocks (in Brazil), two are similar to the bulk of the FLC data ($^{187}Os/^{188}Os_i$ = 0·1273–0·1283). The other two show distinctly higher $^{187}Os/^{188}Os_i$ (0·16–0·184), similar to that (0·1825) of the aliquot of SL10 with low Os concentration.

In summary, geochemical and geochronological data and mineralogical observations demonstrate that the FLC is a high-Ti CAMP occurrence. Isotopically, however, the FLC is distinct with respect to both low-

and high-Ti CAMP rocks (Figs 9–11), constituting a separate isotopic end-member for the CAMP at previously unobserved lower $^{143}Nd/^{144}Nd$ for a given $^{87}Sr/^{86}Sr$ composition, and generally lower $^{206}Pb/^{204}Pb$ and higher $^{207}Pb/^{204}Pb$ and $^{208}Pb/^{204}Pb$.

Isotopic constraints on the petrogenesis of the FLC

Crustal assimilation

The FLC intrudes Archean rocks at mid-crustal depths [3–6 kbar according to Chalokwu *et al.* (1999)]. The first possibility to explore is whether the unusual isotopic characteristics of the FLC derive from assimilation of local crustal rocks, as the large volumes and long residence times of magmas stored in crustal reservoirs favour their contamination by the surrounding country rocks as they cool and differentiate.

Primarily owing to the high $^{207}Pb/^{204}Pb$ of the FLC, we consider that the old (Paleoproterozoic or Archean) terranes of the West African Craton could be potential crustal contaminants. Published isotopic data for the local crust unfortunately are scarce and no data are available for the local Archean rocks (Liberian cycle, *c.* 2·7 Ga). However, a few Sr–Nd isotopic data have been published (Ben Othman *et al.*, 1984; Boher *et al.*, 1992; Deckart *et al.*, 2005) for the Proterozoic terranes (Birimian–Eburnean cycle, *c.* 2·1 Ga) of the basement of Liberia, Guinea and Guyana (the last was juxtaposed to West Africa before Pangea breakup; Abouchami *et al.*, 1990; Skinner *et al.*, 2004; Lytwin *et al.*, 2006). In none of these cases do Pb, Hf or Os isotope data exist for the local continental crust.

Various contaminants (compositional details are given in the caption to Fig. 12), with isotopic compositions recalculated at 200 Ma, were considered: (1) a granodiorite from Guinea (Boher *et al.*, 1992) and (2) a Proterozoic dolerite from Guyana (Deckart *et al.*, 2005), which represent, respectively, silicic and mafic upper crustal end-members; (3) ~~a Liberian~~ lower crustal granulite with very radiogenic $^{87}Sr/^{86}Sr$ (Ben Othman *et al.*, 1984) and (4) a granulite from Guyana with more moderate isotopic characteristics, but strongly enriched incompatible trace element contents (Ben Othman *et al.*, 1984), were taken as representatives of the closest granulitic lower crustal terranes with published isotopic data. Because it is also necessary to consider the effect of assimilation on Pb isotopic compositions, we further took into account (5) Archean granulites from Lashaine, Tanzania (East Africa; Cohen *et al.*, 1984) and (6) Archean granulites from the North China Craton (Ying *et al.*, 2010), as representatives of typical low-$^{206}Pb/^{204}Pb$ ancient granulitic lower crust. Lastly, (7) the noritic, enriched portion of sample SL18, namely SL18N, was considered as the remaining portion of a granulitic xenolith incorporated into the magma chamber, comparable ~~with~~ granulitic enclaves within the FLC reported by Wells (1962) and Hattori *et al.* (1991).

Notably, SL18N has an extreme Pb isotopic composition, which, to the best of the authors' knowledge, is shared by only Lashaine granulites (Tanzanian Craton; Cohen *et al.*, 1984) and plots beyond the already extreme signatures of (1) Archean to Proterozoic mafic granulites [i.e. from Lesotho, South Africa and Eastern Africa; see compilation by Escrig *et al.* (2004)], (2) the 2·3 Ga North China ~~craton~~ (Ying *et al.*, 2010), and (3) the late Archean (2·8–3·0 Ga) Lewisian (Scotland) and Nuk (Greenland) high-grade gneisses (Liew *et al.*, 1991), also known for their very low $^{206}Pb/^{204}Pb$. All these Archean–Proterozoic crustal rocks have $^{206}Pb/^{204}Pb$ and $^{208}Pb/^{204}Pb$ signatures comparable with those of SL18N, but invariably lower $^{207}Pb/^{204}Pb$. We argue that crust such as that represented by SL18N could have been extracted from ancient (up to 3·4 Ga; Lytwin *et al.*, 2006) cratonic lithosphere with high U/Pb (resulting in high time-integrated $^{207}Pb/^{204}Pb$), and high U/Th or low Th/Pb (hence growing in relatively low time-integrated $^{208}Pb/^{204}Pb$), a condition generally achieved in supra-subduction-zone environments. A later melt extraction episode within the lower crust could have caused Rb, U, and Th removal from the restite, resulting in retention of low $^{87}Sr/^{86}Sr$, $^{206}Pb/^{204}Pb$ and $^{208}Pb/^{204}Pb$ at a given $^{143}Nd/^{144}Nd$. Notably, this is not out of context, as a major crust-forming event (the Birimian–Eburnian cycle) occurred in West Africa at *c.* 2·1 Ga (Abouchami *et al.*, 1990; Boher *et al.*, 1992).

We calculated crustal assimilation trends using the assimilation–fractional crystallization (AFC) model of De Paolo (1981), taking as starting composition a basaltic melt ideally derived from the upper, convecting asthenosphere, with the isotopic compositions of DMM, back-calculated to 200 Ma ($^{87}Sr/^{86}Sr = 0{\cdot}70258$; $^{143}Nd/^{144}Nd = 0{\cdot}51283$; Workman & Hart, 2005) and the trace element contents of enriched MORB (Sr = 155 ppm; Nd = 10 ppm; Sun & McDonough, 1989). Because no sampled CAMP rock has picritic or near-primitive compositions, the composition of the parental melt for CAMP basalts must be assumed. Regression-based estimates of primary magma compositions from a compilation of more than 750 CAMP whole-rock major and trace element analyses are available from Salters *et al.* (2003) for intermediate- and low-Ti, but not high-Ti melts. However, our chosen starting composition is similar in major and trace element abundances to the melts calculated by Salters *et al.* (2003), marking it as a reasonable CAMP primary melt.

The only AFC paths that intersect the FLC rocks in Sr–Nd isotope space are those calculated for assimilation of the Guyana lower crustal granulite and the Archean North China Craton granulites (Fig. 12). Assimilation of upper crustal lithologies is therefore ruled out by this model. Starting from the composition of an asthenospheric melt and with $r = 0{\cdot}25$ (a plausible estimate for the ratio between assimilation rate and fractionation rate for a mafic intrusion with a tholeiitic parental magma; Tegner *et al.*, 2005), the FLC rock compositions are reproduced when *F* (the fraction of

J_ID: PETROLOGY Customer A_ID: EGX073 Copyedited by: PR Manuscript Category: Original Article Cadmus Art: O

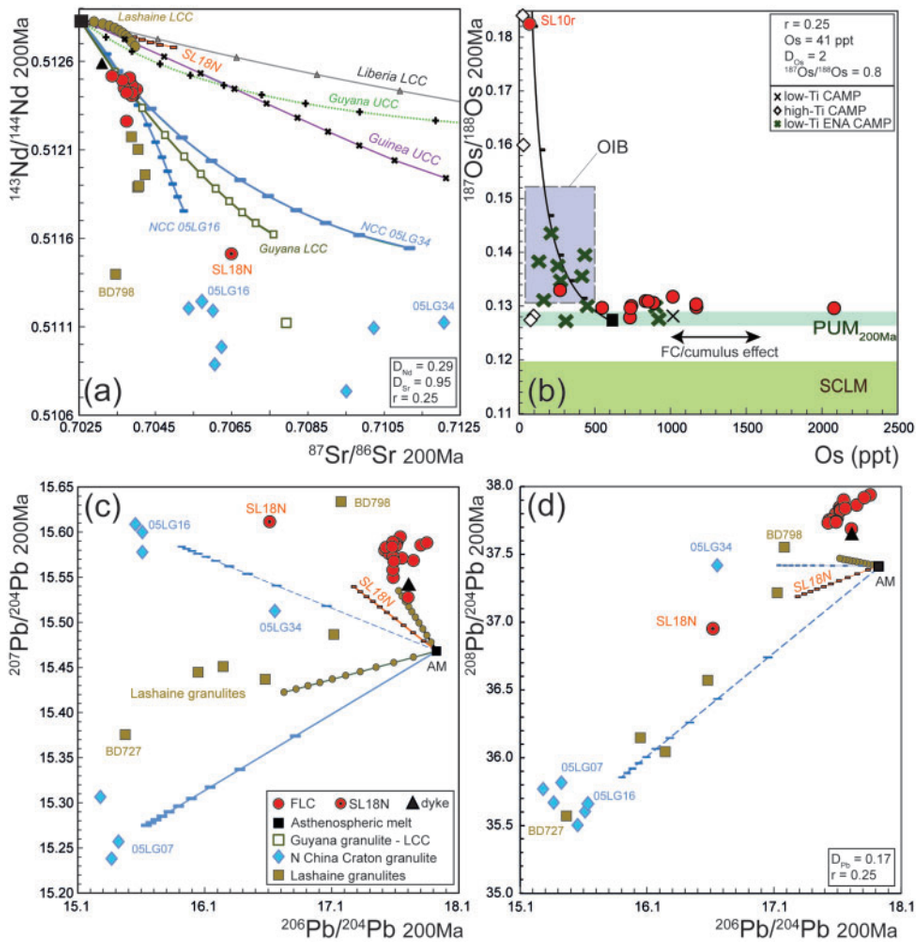

Fig. AFC paths calculated starting from an initial asthenospheric melt (AM; $^{87}Sr/^{86}Sr$ 0·70258, $^{143}Nd/^{144}Nd$ 0·51283, $^{206}Pb/^{204}Pb$ 17·92, $^{207}Pb/^{204}Pb$ 15·47, $^{208}Pb/^{204}Pb$ 37·41, $^{187}Os/^{188}Os$ 0·1272, Sr 155 ppm, Nd 10 ppm, Pb 0·6 ppm, Os 1000 ppt; Workman & Hart, 2005; Dale *et al.*, 2009) for several potential assimilant compositions, recalculated at 200 Ma. (i) A granodiorite from Guinea ($^{87}Sr/^{86}Sr$ 0·713093, $^{143}Nd/^{144}Nd$ 0·510959, Sr 525 ppm, Nd 18 ppm; Boher *et al.*, 1992) as a silicic upper crustal end-member; (ii) a Proterozoic dolerite from Guyana ($^{87}Sr/^{86}Sr$ 0·719879, $^{143}Nd/^{144}Nd$ 0·511811, Sr 166 ppm, Nd 28·87 ppm; Deckart *et al.*, 2005) as a mafic upper crustal end-member; (iii) a Liberian lower crustal granulite with very radiogenic Sr isotopes ($^{87}Sr/^{86}Sr$ 0·7370, $^{143}Nd/^{144}Nd$ 0·5109, Sr 272 ppm, Nd 18 ppm; Ben Othman *et al.*, 1984); (iv) a granulite from Guyana with more moderate isotopic characteristics ($^{87}Sr/^{86}Sr$ 0·70791, $^{143}Nd/^{144}Nd$ 0·51127) but strongly enriched in trace elements (Sr 870 ppm, Nd 65 ppm; Ben Othman *et al.*, 1984); (v) Archean lower crustal granulites from Lashaine (sample BD798: $^{87}Sr/^{86}Sr$ 0·70347, $^{143}Nd/^{144}Nd$ 0·5114, $^{206}Pb/^{204}Pb$ 17·17, $^{207}Pb/^{204}Pb$ 15·63, $^{208}Pb/^{204}Pb$ 37·55, Sr 1333 ppm, Nd 1·83 ppm, Pb 0·93 ppm; and sample BD727: $^{87}Sr/^{86}Sr$ 0·70405, $^{143}Nd/^{144}Nd$ 0·5119, $^{206}Pb/^{204}Pb$ 15·48, $^{207}Pb/^{204}Pb$ 15·38, $^{208}Pb/^{204}Pb$ 35·57, Sr 1226 ppm, Nd 3·72 ppm, Pb 1·37 ppm; Cohen *et al.*, 1984); (vi) the North China Craton (NCC; sample 05LG16: $^{87}Sr/^{86}Sr$ 0·70574, $^{143}Nd/^{144}Nd$ 0·51125, $^{206}Pb/^{204}Pb$ 15·6, $^{207}Pb/^{204}Pb$ 15·6, $^{208}Pb/^{204}Pb$ 35·7, Sr 1279 ppm, Nd 39·5 ppm, Pb 10·8 ppm; and sample 05LG34: $^{87}Sr/^{86}Sr$ 0·71208, $^{143}Nd/^{144}Nd$ 0·51113, $^{206}Pb/^{204}Pb$ 16·65, $^{207}Pb/^{204}Pb$ 15·51, $^{208}Pb/^{204}Pb$ 37·42, Sr 471 ppm, Nd 59 ppm, Pb 2·41 ppm; Ying *et al.*, 2010); (vii) the noritic, enriched portion of sample SL18, namely SL18N ($^{87}Sr/^{86}Sr$ 0·7065, $^{143}Nd/^{144}Nd$ 0·511515, $^{206}Pb/^{204}Pb$ 16·61, $^{207}Pb/^{204}Pb$ 15·61, $^{208}Pb/^{204}Pb$ 36·95, Sr 351 ppm, Nd 3·71 ppm, Pb 1·41 ppm), interpreted as the remaining portion of a granulitic xenolith incorporated into the magma chamber. All the curves are calculated for $r = 0{\cdot}25$ (where r is ratio of mass assimilation rate to fractional crystallization rate). Tick marks are placed every $F = 0{\cdot}1$ from $F = 1$ to $F = 0$ (where F is fraction of magma remaining). From the initial magma (AM), tick marks indicate *c.* 3·3, 6·7, 8·3, 10·7, 16·7, 20, 23, 27 and 30 wt % M_a (where M_a is mass assimilated), calculated for $r = 0{\cdot}25$. $^{187}Os/^{188}Os$ data for previously analysed CAMP rocks are from Merle *et al.* (2011, 2014) and Callegaro *et al.* (2013, 2014).

magma remaining) is between 0·9 and 0·8 (bulk partition coefficient D = 0·29 for Nd and 0·95 for Sr). To reach FLC-like Sr–Nd isotopic compositions from the asthenospheric parental melt, incorporation of between 4 and 7 wt % lower crustal granulite appears sufficient (same parameters as above).

We estimate that at 200 Ma the $^{187}Os/^{188}Os$ of such local lower crust (Os = 41 ppt) would range between 0·8 and unity, assuming that this crust was extracted from the PUM at 2 or 3 Ga and evolved with a lower crustal $^{187}Re/^{188}Os$ ratio of *c.* 20 [lower crustal and PUM parameters as given by Saal *et al.* (1998) and Meisel *et al.* (2001)]. The initial asthenospheric melt is assigned an $^{187}Os/^{188}Os$ composition of 0·1272, which is that estimated for the convective mantle (Dale *et al.*, 2009) corrected to 200 Ma, but the value of the PUM (0·128 at 200

AQ6 Ma; Meisel *et al.*, 2002) can alternatively be used with no substantial difference in the modeling results. In tholeiitic basalts with low Os contents, assimilation of old crustal rocks with highly radiogenic compositions will rapidly modify the initial Os isotopic ratios. However, with two exceptions (samples SL10 and SL38), the FLC rocks have Os whole-rock concentrations ranging from 550 ppt to ~1200 ppt, suggesting that these cumulates formed from Os-rich melts. The exact Os concentrations of these melts depend on the D_{Os} value, which is difficult to constrain. Nevertheless, given the near absence of sulphides, silicate–melt partitioning is likely to control Os concentrations in the magma. Analogy with the olivine–melt partition coefficients of Ru and Ir (Brenan *et al.*, 2016), two PGEs similar to Os, suggests that a D_{Os} value of ~2 is a reasonable choice, implying that the FLC rocks were in equilibrium with melts containing about 300–600 ppt Os. AFC calculations then show that the $^{187}Os/^{188}Os$ ratios of most samples would not be strongly perturbed by the addition of up to 7 wt % granulitic lower crust (as constrained by the Sr–Nd isotopic systems); that is, $^{187}Os/^{188}Os$ increases from 0·1272 to *c.* 0·132, considering a total $D_{Os} = 2$ and an $r = 0{\cdot}25$, starting from an initial Os content of 600 ppt for the asthenospheric starting melt. It should be noted that 600 ppt is a minimum concentration for the initial asthenospheric melts, as some fractional crystallization may have occurred prior to emplacement of the magmas in the FLC or in unexposed layers of the complex. Higher initial Os concentrations would imply even stronger immunity to the effects of crustal contamination.

Whereas most of the samples seem unaffected by crustal contamination, this process has substantially modified the Os isotopic composition of one aliquot of sample SL10 (Table 4), which has an initial $^{187}Os/^{188}Os$ of 0·182 ± 0·005, coupled with an Os concentration of 0·068 ppb. Evidence for crustal contamination in this sample is not surprising given its highly differentiated nature (MgO = 3·54 wt %, by far the lowest value of all the samples analysed for Os isotopes) and its relatively high $^{87}Sr/^{86}Sr$ (0·70402). A slight hint of crustal contamination may also be present in sample SL38 ($^{187}Os/^{188}Os$ = 0·133 ± 0·005), which has the second lowest Os concentration (0·270 ppb) as well as the second lowest MgO content (7·35 wt %). Previous evidence for crustal contamination based on Os isotopes during ~~the~~ late stages of differentiation was provided by Hattori *et al.* (1991), who determined $^{187}Os/^{188}Os_i$ values up to 0·253 in magmatic PtFe alloys collected in eluvial deposits above zone 3 of the FLC, the zone from which SL10 was collected. In addition to these radiogenic PtFe alloys, Hattori *et al.* (1991) found ehrlichmanite (OsS_2) nuggets with $^{187}Os/^{188}Os$ (0·130–0·132) indistinguishable from those of nearly all of the present FLC samples. The heterogeneous distribution of such nuggets probably explains why the other aliquot of SL10 has an exceptionally high Os concentration (2·080 ppb) coupled with low $^{187}Os/^{188}Os_i$ (0·1296 ± 0·0010).

Although Os isotopes do show evidence for crustal contamination in one or two samples, they offer few constraints on the process. Instead, the critical clue for determining the importance of crustal contamination is provided by Pb isotopes. It is not possible to reproduce the $^{207}Pb/^{204}Pb$ and $^{208}Pb/^{204}Pb$ characteristics of the FLC rocks by addition of 7 wt % Archean lower crustal granulites (whether from Guyana or the North China Craton) starting from a DMM initial composition. Assimilation of the more isotopically extreme Lashaine granulites also does not reproduce the Pb isotope compositions, which was already excluded by AFC modeling of the Sr and Nd isotope systematics. No lower crustal composition can be found in the literature that, when assimilated by an asthenospheric parental melt (using the *r* and *F* values constrained by the Sr–Nd isotope systems), would lever up the Pb isotopic composition enough to produce the signatures shown by the FLC. Therefore, even if the Os isotope characteristics of some samples (SL10r and SL38), as well as the interpretation of SL18N as a lower crustal xenolith, suggest that some lower crustal assimilation affected the FLC magma, the AFC calculations show that this was a minor process. Crustal contamination may be responsible for some of the compositional variability observed within the cluster of the FLC data, but not for their unusual Pb isotopic signature (primarily the high Δ7/4 and Δ8/4). Hence, the process that shifted the Pb isotope compositions of these mantle-derived melts must be sought within their mantle source.

It is of some interest to compare the effects of crustal contamination in the FLC with those in the ore-bearing Noril'sk and Talnakh mafic intrusions (Russia), which similarly to the FLC are related to the activity of a Large Igneous Province (the Siberian Traps). Although the FLC displays some PGE enrichment, it is not comparable with the economic deposits found at Noril'sk and Talnakh. In particular, in the Siberian intrusions, the sulphur hosted by the massive and disseminated sulphide mineralization rich in Cu–Ni–PGE has been demonstrated to be of crustal origin on the basis of S isotopes (Ripley *et al.*, 2003). Whereas Noril'sk and Talnakh intruded evaporitic sediments, the FLC intruded crystalline basement whose metamorphic lithologies are not readily assimilated or contact metamorphosed, as also demonstrated by our AFC calculations.

Enriched lithospheric source

Isotopic compositions such as those observed for the FLC (i.e. their position to the left of the Geochron at high Δ7/4 and high Δ8/4) call for the involvement of an ancient (i.e. Archean) reservoir in their formation. Ancient domains are present in the peri-cratonic geodynamic setting of the FLC, which intruded a Panafrican (Neoproterozoic) orogenic belt that deformed Archean crustal rocks (aged from 3·4 to 2·8 Ga; Lytwin *et al.*, 2006). Osmium and Hf isotopes exclude a dominant contribution from wholesale melting of the residual

sub-continental lithospheric mantle (SCLM), because a depleted SCLM would have imparted low $^{187}Os/^{188}Os$ and $^{176}Hf/^{177}Hf$ signatures to the FLC magmas ($^{187}Os/^{188}Os$ lower than 0·125 and negative ε_{Hf} values, down to –55; Griffin *et al.*, 2000; Carlson *et al.*, 2005; Choukroun *et al.*, 2005), which are not observed in our samples. Also, such a residual mantle would be unlikely to melt in the absence of an important thermal anomaly (e.g. a mantle plume) because of being cold, refractory, and depleted in magmaphile major elements (e.g. Carlson *et al.*, 2005; O'Reilly *et al.*, 2009). Finally, isotopic compositions such as those of the FLC are unknown among OIB, even among those with a significant EMI signature. This makes OIB sources unlikely for the FLC magmas.

Fertile domains within the SCLM can instead be the conveyors of the unusual FLC isotopic signatures. The presence of metasomatized portions in the lithospheric mantle below Sierra Leone in particular and Western Africa in general is reflected by widespread occurrences of both sodic and potassic alkaline magmatic bodies, varying in age from Neoproterozoic to Mesozoic. In particular, lamproites are found in Bobi (Ivory Coast; Cretaceous; Pouclet *et al.*, 2004) and several kimberlitic pipes punctuate the Man Craton (Neoproterozoic to Jurassic; Skinner *et al.*, 2004), the nearest of which crop out at Koidu–Tongo (Sierra Leone; Taylor *et al.*, 1994) and Godua–Kumgbo (Liberia), *c.* 250 km east and SE of Freetown, respectively. Kimberlites have also been reported in southeastern Guinea (Droujba–Bouro–Banankoro clusters; Skinner *et al.*, 2004) and in southwestern Mali (Kenieba; Taylor *et al.*, 1994) and on the once nearby Guyana craton (Guaniamo, Venezuela; Kaminski *et al.*, 2004). Finally, occurrences of nepheline syenites and carbonatites have been reported in the Rokelide belt (Burke & Webb, 2003; Lytwin *et al.*, 2006).

AQ7

Only eclogitic mantle xenoliths entrained by the Koidu kimberlites (Tibbetts, 2010) from Sierra Leone have been characterized isotopically. The extremely variable signatures of these eclogites bracket, but do not match, those of the FLC (Supplementary Data Fig. 5). No isotopic data have been published for local lamproitic rocks, mainly because of their severe state of alteration (Pouclet *et al.*, 2004). Following the definition of Nelson (1992), anorogenic lamproites are confined to the margins of stable cratons and have isotopic characteristics distinct from those of 'orogenic' lamproites (associated with young orogenic belts or active continental margins). Although lamproitic rocks from different localities have distinct signatures, anorogenic lamproites from worldwide circum-cratonic settings all share some common Pb isotopic features; that is, low $^{206}Pb/^{204}Pb$ and variably high $^{207}Pb/^{204}Pb$ and $^{208}Pb/^{204}Pb$ (e.g. Gaussberg, Western Australia, Leucite Hills, and Alto Paranaíba lamproites; Fraser *et al.*, 1985; Bergman, 1987; Nelson, 1992; O'Brien *et al.*, 1995; Murphy *et al.*, 2002; Mirnejad & Bell, 2006; Carlson *et al.*, 2007). With a few exceptions, the enriched subcontinental lithospheric mantle has been recognized as the most likely mantle source of anorogenic lamproites. A possible scenario for the genesis of the lamproites requires a multi-phase history for their mantle source, starting with (ultra)depletion of the SCLM followed by later metasomatism, either in a suprasubduction-zone context or produced by melts ascending from the asthenosphere. To achieve time-integrated enrichment of radiogenic isotopes, lamproite formation should occur only after long residence of the metasomatic veins within the SCLM (Bergman, 1987; Mitchell & Bergman, 1991; Nelson, 1992; Prelević *et al.*, 2010; Kononova *et al.*, 2011). We suggest that SCLM metasomatic veins similar to the source rocks of anorogenic lamproites may have acted as enriched contributors in the genesis of the FLC because (1) they are the only known repository of isotopic signatures as extreme as those observed in our samples (low $^{206}Pb/^{204}Pb$ and variably high $^{207}Pb/^{204}Pb$ and $^{208}Pb/^{204}Pb$) and (2) the setting of the FLC in a cratonic margin environment is suitable for the occurrence of metasomatic veins and their ~~long~~ preservation within stable and cold cratonic keels.

Modeling

Here we try to reproduce the isotopic signatures of the FLC by mixing upper asthenospheric melts with small volumes of lamproitic melts derived from metasomatized lithospheric mantle. A similar origin (i.e. hybridization of high-degree asthenospheric melts with small volumes of lithospheric alkaline melts) has also been suggested for Karoo (Ellam & Cox, 1991; Heinonen *et al.*, 2016) and Paraná (Gibson *et al.*, 1995) continental flood basalts (CFB).

The lithophile (Sr–Nd–Pb–Hf) isotopic systems are controlled by enriched silicate melts, whereas the Re–Os isotopic system is not. Primary asthenospheric melts are likely to be Os-rich (1000–1600 ppt Os; see Dale *et al.*, 2009), if the degree of melting is high enough to dissolve sulphides (the main host of Os in mantle peridotites). The broadly PUM-like (~0·128 at 200 Ma; Meisel *et al.*, 2001) or slightly less radiogenic (Dale *et al.*, 2009) Os isotopic composition (i.e. $^{187}Os/^{188}Os \sim 0{\cdot}127$ at 200 Ma) of such asthenospheric melts would thus remain nearly unchanged by addition of a small volume of melt that is likely to have a more radiogenic Os isotope composition (highly alkaline rocks from Brazil: $^{187}Os/^{188}Os_{85Ma}$ up to 0·30, Carlson *et al.*, 1996; highly alkaline rocks from India: $^{187}Os/^{188}Os_{1300Ma}$ up to 0·55, Chalapathi Rao *et al.*, 2013), but with a much lower Os concentration (0·02–0·6 ppb, Carlson *et al.*, 1996; 0·08–0·13 ppb, Chalapathi Rao *et al.*, 2013).

As discussed above, ~~cumulus~~ effects in the FLC rocks ~~strongly~~ hinder the use of whole-rock trace element abundances in petrogenetic modeling ~~and the composition of parental CAMP melts~~ must be assumed (see the section on crustal assimilation). The chosen parental melt is produced by *c.* 10–12% modal batch melting of the upper asthenosphere (see Heinonen *et al.*, 2016) with the Sr–Nd–Hf–Pb isotopic signatures of the DMM

Table 5: Isotopic and trace element compositions (all in ppm, except for Os in ppt) of the mixing end-members (asthenospheric melt and lamproitic melt) for the source modeling

	Asthenospheric melt	Lamproitic melt
Sr	155	1218
Nd	10	236
Pb	0·6	30
Hf	2·05	20·7
Os (ppt)	1000	500
$^{87}Sr/^{86}Sr$	0·70258	0·7110
$^{143}Nd/^{144}Nd$	0·5128	0·5117
ε_{Nd}	+8·19	−13·28
$^{187}Os/^{188}Os$	0·1272	0·380
$^{176}Hf/^{177}Hf$	0·28306	0·28194
ε_{Hf}	+14·58	−25·05
$^{206}Pb/^{204}Pb$	17·92	17·30
$^{207}Pb/^{204}Pb$	15·47	15·68
$^{208}Pb/^{204}Pb$	37·41	38·30

Sr and Nd concentrations are from the Bobi lamproite, the nearest available lamproite occurrence (Pouclet et al., 2004). Sr–Nd–Pb–Hf concentrations and isotope compositions are within the range observed for Western Australia lamproites. Osmium, the least well constrained, is within the range of Brazilian alkaline magmatism (Carlson et al., 1996) and Krishna lamproites (Chalapathi Rao et al., 2013). Isotopic signatures of the asthenospheric melt are back-calculated to 200 Ma, whereas those of the lamproitic melt are not.

(see Table 5 for values and references). The Os concentration and isotopic composition are chosen to be representative of an upper asthenospheric melt (1000 ppt [Os]; $^{187}Os/^{188}Os = 0·1272$; Dale *et al.*, 2009; Table 5). A deep mantle melt would ideally have the isotopic signature of the so-called PREMA (Prevalent Mantle; Zindler & Hart, 1986) reservoir, whose Sr isotopic signature ($^{87}Sr/^{86}Sr$ *c.* 0·7035) is already too radiogenic compared with that of the least evolved of our samples. It is also worth noting that taken together, the available Pb isotopic data for the CAMP form a large field (see Fig. 10a) with one vertex pointing toward the DMM end-member, thus suggesting that the upper depleted asthenosphere is the common mantle source for this LIP. For the high-Ti suite in particular, involvement of a high-$^{206}Pb/^{204}Pb$ component, such as FOZO or C (Hart *et al.*, 1992; Hanan & Graham, 1996; Stracke *et al.*, 2005), dominant among Atlantic OIB, seems unlikely. However, the present ~~dataset~~ cannot conclusively distinguish between a deep and a shallow asthenospheric provenance for the main magma batch. In contrast, it confirms the involvement of an ancient strongly enriched component.

The upper asthenospheric parental melt is mixed with an ultra-alkaline melt (Table 5) with Sr–Nd–Hf–Pb isotopic and trace element compositions within the field defined by worldwide anorogenic lamproites (Figs 9 and 10; Bergman, 1987; Mitchell & Bergman, 1991; Nelson, 1992; Prelević *et al.*, 2010). Notably, although all worldwide anorogenic lamproites have low $^{206}Pb/^{204}Pb$, each occurrence is characterized by a unique signature with high, but variable $^{207}Pb/^{204}Pb$ and $^{208}Pb/^{204}Pb$. Hence, the composition chosen here as mixing end-member is not meant to represent a particular lamproitic province, but rather a plausible composition for the local enriched domains in the SCLM below Sierra Leone. In this sense, the small isotopic variability within our ~~dataset~~ could be due to (minor) amounts of assimilation of local granulites (see AFC trajectories in Figs 9 and 12), but also, as Ellam & Cox (1991) pointed out for picrites from the Karoo LIP, to isotopic heterogeneities in different batches of enriched lithospheric melt added to the original asthenospheric melt. Not only are lamproites heterogeneous on a worldwide scale, but being low-degree melts of anomalously enriched portions of the SCLM, they are likely to be heterogeneous ~~even~~ at the local scale.

For the Os isotopic compositions of the enriched lithospheric melt component, we chose average values representative of the Alto Paranaìba lamproites (Carlson *et al.*, 2007). However, we emphasize that whatever the chosen Os isotopic signature for the lamproite, the Os budget and Os isotopic composition would be efficiently buffered by the asthenospheric melt. Only a massive lamproitic contribution would be able to shift the PUM-like signature towards significantly more or less radiogenic values (Carlson *et al.*, 2007; Rocha-Júnior *et al.*, 2012), but if this were the case, the major and trace element contents of the asthenospheric melt would also be affected, as ultra-alkaline magmas are extremely enriched in lithophile incompatible trace elements. Such effects are not observed for the FLC samples. It is also important to note that even a very small lamproitic addition (*c.* 1–3%, calculated based on simple binary mixing) to a depleted asthenospheric melt is able to modify its Sr, Nd, Pb and Hf isotopic compositions to resemble those observed for the FLC.

If mixing of a dominant asthenospheric melt with low-volume melts derived from enriched veins in the SCLM occurred, a certain spectrum of values in the resulting enrichment would be expected in the ~~dataset~~. This, however, is not the case. The FLC magmas, despite being emplaced in four zones (each representing different pulses), appear essentially as a single batch of magma, very homogeneous in composition and modified only by some very minor crustal contamination *in situ* (compare SL18N and SL10). There is general agreement that most CFBs pond in large magma chambers within the deep crust or at the Moho, where homogenization can take place (Black & Manga, 2017; Jennings *et al.*, 2017). This could explain the compositional homogeneity characterizing the FLC; that is, within a deep magma chamber, efficient mixing occurred between melts with a ~~dominant~~ DMM signature and strongly enriched lamproitic melts derived from the SCLM. This scenario also is consistent with what is observed in other CAMP regions (e.g. in North America and Morocco), where samples from distinct flows but from the same unit or lava formation (e.g. Orange to Hook Mountain and Lower to Recurrent, respectively) are essentially identical in composition.

THE FREETOWN LAYERED COMPLEX VIEWED IN THE BROADER CONTEXT OF MANTLE ENRICHMENT

Implications for the mantle source of high-Ti magmas of circum-Atlantic Gondwana LIPS

The inferred involvement of enriched SCLM in the genesis of the high-Ti magmas of the FLC may be linked to the tectonic setting of the intrusion. The location of the FLC on a cratonic margin may explain its distinct isotopic characteristics (particularly its Pb isotopic composition; Fig. 10) with respect to other CAMP occurrences. CAMP high-Ti magmas crop out only in a restricted area, between the western border of the Man Craton and the eastern border of the Amazonian Craton. As already inferred for the Maranhão (Parnaiba basin) high-Ti CAMP basalts from NE Brazil (Merle *et al.*, 2011), a contribution from melts derived from metasomatized portions of the lithosphere is the simplest interpretation of the isotopic signatures of the high-Ti FLC magmas. Likewise, high-Ti basalts from other LIPs, such as the Paraná–Etendeka (Rocha-Júnior *et al.*, 2013) and the Karoo (Jourdan *et al.*, 2007), are geographically limited and generally adjacent to cratonic areas, and in particular are found along continental edges or in major mobile belts. These structures, often cutting through crust and mantle lithosphere and extending down to the asthenospheric mantle, could serve as preferential channels for rising mantle melts and may represent sites of enriched lithospheric domains (Jourdan *et al.*, 2006). As pointed out by Carlson *et al.* (1996), magmatism of EMI-like nature is not restricted to intra-plate domains (OIB), but also occurs in (Proterozoic) mobile belts surrounding (Archean) cratons, and, in general, magmatism spatially associated with Proterozoic mobile belts often has elevated Ti contents (Gibson *et al.*, 1995). This is the case for the high-Ti Cretaceous alkaline magmatism and high-Ti Paraná CFBs, closely associated with Middle to Late Proterozoic mobile belts surrounding the São Francisco and Amazonas cratons in the Paraná basin (Gibson *et al.*, 1995; Carlson *et al.*, 1996; Comin-Chiaramonti *et al.*, 1997, 2007). It is also the case for high-Ti magmatism from southern Africa, where both the high-Ti alkaline rocks and the high-Ti CFBs of the Karoo LIP occur in close spatial association with Proterozoic mobile belts (respectively, the Damara and Kibaran belts, bordering the Congo craton and between the Kaapvaal and the Zimbabwe cratons; Ellam & Cox, 1991; Gibson *et al.*, 1995; Jourdan *et al.*, 2007). A similar pattern is visible for the Cenozoic potassic alkaline suite emplaced around the edges of the Wyoming craton (O'Brien *et al.*, 1995) and for the Virunga high-Ti alkaline magmas from Proterozoic domains in East Africa (Gibson *et al.*, 1995). The model presented here for the genesis of the FLC seems to fit well into this global pattern. Continental lithosphere with the general isotopic characteristics of EMI is apparently produced at destructive margins during the formation of mobile belts around cratons by infiltration of alkalic melts (Carlson *et al.*, 1996). These enriched domains, secluded within mobile belt lithosphere, could be fertile and prone to melting during later (e.g. LIP-related) thermo-tectonic events. Therefore, in the case of the CAMP, Karoo and Paraná–Etendeka LIPs, the spatial distribution and distinct geochemical features of the high-Ti magmas suggest lithospheric control on magma composition and distribution. The restricted spatial distribution of high-Ti basalts thus would reflect preferential areas of lithospheric contamination of asthenosphere-derived melts rather than the superficial expression of impinging mantle plumes.

Nevertheless, arguments can also be made in favour of a deep mantle origin for the CAMP volcanism. In particular, Puffer (2001) proposed a model for distinguishing plume from reactivated-arc sources for CFBs, based on high field strength element systematics. Following this model, the vast majority of CAMP (low-Ti) magmas would result from reactivation of a back-arc source during decompression associated with continental breakup (Puffer, 2003), whereas the smaller, localized high-Ti portion of the CAMP would arise from the impingement of a mantle plume. This hypothesis, based exclusively on trace element data, is difficult to test on the FLC cumulate rocks. Only the dyke's trace element composition partially supports OIB affinity, albeit with some differences in K, Nb, Ta, Pb, Sr, Zr, and Hf abundances. However, the extreme isotopic composition of the FLC and the dyke is different from any known OIB composition. Although we cannot completely rule out a contribution from a mantle plume, an OIB-like source is not required to reproduce the observed FLC isotopic composition. Rather, the data are readily reproduced by the scenario proposed above, involving a predominantly asthenospheric (DMM) origin followed by subsequent enrichment from interaction with enriched portions within the cratonic SCLM. In this sense, it is intriguing that high-Ti basalts were formed only in a relatively restricted area close to the Man, Guyana and Amazonian cratons, which were sites of abundant ultra-alkaline magmatism.

Torsvik *et al.* (2010) demonstrated through paleomagnetic reconstructions that the present-day positions of active hotspots and the reconstructed locations of large igneous provinces are focused along the margins of Large Low Shear Velocity Provinces (LLSVP; Burke *et al.*, 2008), inferring that the LLSVPs are stable, long-lasting, thermochemical regions at the base of the lower mantle. The steep sides of the LLSVPs may deflect and channel upwards hot material sweeping the lower mantle, hence behaving as plume generation walls. In 200 Ma plate reconstructions (Ruiz-Martínez *et al.*, 2012) Sierra Leone is ~~indeed~~ located above the margin of the African LLSVP, as is the Karoo at *c.* 183 Ma and the Paraná–Etendeka at *c.* 135 Ma (see Svensen *et al.*, 2017). It is not yet clear if the nature of the LLSVPs is predominantly thermal or thermochemical. As the margin of the LLSVP would underlie a belt stretching from northern Brazil and Sierra Leone to southeastern

Canada and Morocco, it would be expected to generate geochemically similar magmas. This is, however, not observed, as, for example, FLC rocks and Brazilian high-Ti basalts (Merle *et al.*, 2011) are clearly different from Carolina dykes (Callegaro *et al.*, 2013; Whalen *et al.*, 2015) and northeastern USA and Moroccan low-Ti basalts (Bertrand *et al.*, 1982; Merle *et al.*, 2014). Thus, although we cannot rule out thermal input from the African LLSVP in the genesis of the FLC and the CAMP in general, we can rule out that this deep-seated mantle domain imparted a uniform geochemical signature to the entire CAMP, because a uniform signature is not observed. We stress again that the ~~dataset~~ presented here cannot be used to distinguish conclusively between a deep and a shallow asthenospheric source for the parental FLC melt, but it clearly shows that some enrichment process occurring in the lithosphere superimposed its geochemical signature on these ~~particular~~ CAMP magmas.

Enriched DUPAL–LOMU signatures: shallow or deep mantle heterogeneities?

A belt of OIB (e.g. Tristan da Cunha, Inaccessible, and Gough Islands), MORB (e.g. at 26°S in the Atlantic), and seamount chains (e.g. Discovery Seamounts, Walvis Ridge and Rio Grande Rise, South Atlantic) that stretches from the South Atlantic Ocean to the Indian and Pacific Oceans between 0 and 60°S latitude is characterized by high Δ7/4 and Δ8/4 and relatively high $^{87}Sr/^{86}Sr$ (>0·7035; Gibson *et al.*, 2005; Meyzen *et al.*, 2005; Regelous *et al.*, 2009; Salters & Sachi-Kocher, 2010; Class & Le Roex, 2011; Schwindrofska *et al.*, 2016); this signature is referred to as the DUPAL anomaly (Dupré & Allègre, 1983; Hart, 1984; Fig. 13). Another mantle reservoir known as LOMU (low-μ; Douglass *et al.*, 1999; Kamenetsky *et al.*, 2001) has been hypothesized to be the conveyor of these signatures. The origin of the DUPAL–LOMU large-scale mantle heterogeneity

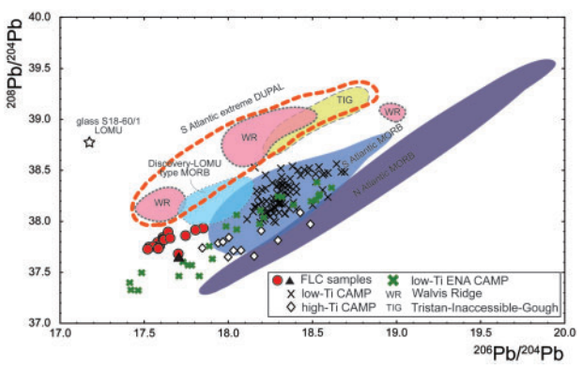

Fig. 13. Pb isotopic data for the FLC (excluding SL18) and low-Ti and high-Ti CAMP rocks (all back-calculated to 200 Ma) plotted together with Atlantic basalts (MORB and OIB; present-day values) showing a DUPAL anomaly (modified after Class & Le Roex, 2011). Plotted also is the composition of the andesitic glass S18-60/1 dredged in the South Atlantic by Kamenetsky *et al.* (2001).

is controversial and has been attributed to either deep mantle plume activity (e.g. Castillo, 1988; Class & Le Roex, 2011; Wen, 2006) or lithospheric (lower crustal or SCLM) recycling in the shallow mantle (Rehkämper & Hofmann, 1997; Kamenetsky *et al.*, 2001; Escrig *et al.*, 2004, 2005; Hanan *et al.*, 2004; Gibson *et al.*, 2005; Meyzen *et al.*, 2007; Regelous *et al.*, 2009; Salters & Sachi-Kocher, 2010).

The data presented here for the FLC show a broadly DUPAL- or LOMU-like isotopic enrichment, which is most easily explained by the involvement of enriched mantle material with the isotopic signature of worldwide anorogenic lamproites. These are in turn commonly thought to be derived from, and thus reflect the isotopic composition of, the enriched SCLM (e.g. Bergman, 1987; Mitchell & Bergman, 1991; Nelson, 1992; O'Brien *et al.*, 1995; Nowell *et al.*, 2003; Carlson *et al.*, 2007; Prelević *et al.*, 2010)—even if in rare cases a deep mantle source has also been evoked (Murphy, 2002). Notably, EMI-like signatures with low $^{206}Pb/^{204}Pb$, high $^{207}Pb/^{204}Pb$, and low $^{143}Nd/^{144}Nd$, coupled with mildly radiogenic $^{87}Sr/^{86}Sr$, are common in alkaline rocks from western Africa and eastern South America, such as, for example, the Cretaceous alkaline magmatism of Brazil (kimberlites, kamafugitic diatremes, carbonatitic complexes; Bizzi *et al.*, 1995; Carlson *et al.*, 1996, 2007). In particular, Bizzi *et al.* (1995) observed that EMI-like signatures are concentrated in the lithospheric portions of the mantle beneath the São Francisco craton. Cretaceous mafic–potassic magmas from SW Africa and eastern South America also trend towards the EMI mantle end-member (Gibson *et al.*, 2005) and have been interpreted as being derived from metasomatized SCLM. These data support the presence of EMI-like domains in the SCLM of the continents surrounding the Central and South Atlantic.

The data presented here for the FLC support the interpretation of the DUPAL and LOMU signatures as typical of ancient metasomatized SCLM and are consistent with previously discussed interpretations for the origin of high-Ti basalts from the Paraná–Etendeka and the Karoo LIPs (e.g. Jourdan *et al.*, 2007; Rocha-Júnior *et al.*, 2012), as well as the Discovery Seamounts (Schwindrofska *et al.*, 2016). Nevertheless, the FLC data cannot resolve whether these enriched signatures are stored in the shallow or the deep mantle. Ancient lithosphere delaminated during the breakup of Gondwana is a likely carrier of the DUPAL–LOMU signature. Lithospheric strands in the upper mantle have been identified by both geochemical (Cape Verde; Escrig *et al.*, 2005; Coltorti *et al.*, 2010) and geophysical (O'Reilly *et al.*, 2009) ~~means~~, and found to be scattered randomly throughout the Atlantic basin. LOMU ideally represents remnants of lithospheric material (SCLM or lower crust) trapped in the oceanic upper mantle after the breakup of Gondwana. Interestingly, Kamenetsky *et al.* (2001) ~~dredged an andesitic~~ glass from the South Atlantic Ridge that closely matches the LOMU isotopic characteristics (Figs 9 and 10), confirming its existence.

The enriched (lamproitic) melts trapped by the dominantly asthenospheric FLC parental melt while ascending through the SCLM of the Man craton have a signature close to that of the LOMU glass (S18-60/1) analysed by Kamenetsky *et al.* (2001). A shallow origin of the DUPAL signature from strands of Gondwana SCLM in the upper mantle is also suggested by the fact that this signature is common in the southern hemisphere and essentially non-existent elsewhere (with a few exceptions, e.g. the Gakkel Ridge; Goldstein *et al.*, 2008). In this sense, it is difficult to assess the validity of a deeply rooted origin for the DUPAL anomaly; if this were the case, any expression of magmatism related to LLSVP margins should display a DUPAL signature, a feature that is not observed.

However, although the FLC data serve as a proxy supporting an ancient enriched SCLM origin for the DUPAL and LOMU signatures, any attempt to further infer shallow or deep storage of these mantle reservoirs would be purely speculative.

CONCLUDING REMARKS

Although the Freetown Layered Complex (FLC) in Sierra Leone has been the object of detailed petrographic, petrological, and some geochemical investigations in the past, an in-depth study of its radiogenic isotope geochemistry and geochronology has long been lacking. The new ages and mineral chemistry data presented here for the FLC demonstrate its affiliation with the Central Atlantic Magmatic Province (CAMP) and its high-Ti character. The new Sr–Nd–Pb–Os isotopic compositions ~~that form part of~~ this study are markedly different from those of the low-Ti CAMP rocks, and more extreme than those of other high-Ti CAMP rocks, thus identifying the FLC as a new CAMP isotopic end-member. Hafnium isotopic compositions for the FLC were ~~also~~ measured and are the first that we are aware of reported for the CAMP. These data further assist in defining the FLC end-member within the CAMP and, more generally, expand on the so-far scarce Hf isotope systematics of continental LIP basalts (e.g. Jourdan *et al.*, 2007). Radiogenic isotope compositions of the FLC are enriched, with EMI-like signatures typical of DUPAL-like circum-Atlantic magmatism, trending towards high $^{207}Pb/^{204}Pb$ at low $^{206}Pb/^{204}Pb$. This peculiarity is shared by anorogenic lamproites worldwide. Minor local interaction with the granulitic lower crust can account for a small part of the isotopic variability displayed by the FLC, but no known crustal composition is able to enrich the isotopic signatures of any mantle melt to the point of reaching the observed FLC isotopic ~~composition.~~ We calculated that a limited (1–3%) contribution of extremely alkaline (lamproitic) melt derived from fertile domains of ancient SCLM is the most straightforward way to imprint the observed signatures on a predominantly asthenospheric melt. The presence of kimberlites and lamproites along the southwestern rim of the West African Craton ~~strengthens~~ this explanation, as well as the fact that ~~they~~ are the only reservoirs with such extreme Pb isotope characteristics. The emplacement of the FLC within a Proterozoic mobile belt that borders a craton suggests that enriched, readily fusible domains were probably present in the underlying lithosphere, a scenario also proposed for other LIPs, such as the Karoo and the Paraná–Etendeka. Enriched signatures (EMI, DUPAL, LOMU) are rather common in oceanic and continental basalts around the South Atlantic Ocean. Our data on the FLC support the origin of these heterogeneities from ancient enriched SCLM domains derived from Gondwana during previous continental breakup, but cannot distinguish between a shallow ~~and~~ a deep origin for this signature.

ACKNOWLEDGEMENTS

We thank R. Carampin for EMP analyses, P. Capiez for XRF analyses and Catherine Zimmermann for assistance with Os analyses. We thank John H. Puffer, Dougal A. Jerram and Gregory McHone for their detailed and helpful reviews, and acknowledge the editorial work of John Gamble.

FUNDING

A.M. acknowledges financial support from CARIPARO (Eccellenza 2008), Progetto di Ateneo 2013 (Università di Padova, CPDA132295/13), and PRIN (20158A9CBM). H.B. acknowledges financial support from CNRS-INSU (program SEDIT). J.B.T. acknowledges financial support from the French Agence Nationale de la Recherche through ~~the~~ grant ANR-10-BLANC-0603 M&Ms—Mantle Melting—Measurements, Models, Mechanisms. Osmium isotopic analyses were financed by the Europlanet program.

SUPPLEMENTARY DATA

Supplementary data for this paper are available at *Journal of Petrology* online.

REFERENCES

Abouchami, W., Boher, M., Michard, A. & Albarède, F. (1990). A major 2·1 Ga event of mafic magmatism in west Africa: An early stage of crustal accretion. *Journal of Geophysical Research* **95**, 17605.

Beckinsale, R. D., Bowles, J. F., Pankhurst, R. J. & Wells, M. K. (1977). Rubidium/strontium age studies and geochemistry of acid veins in the Freetown complex, Sierra Leone. *Mineralogical Magazine* **41**, 501–511.

Bédard, J. H. (2014). Parameterizations of calcic clinopyroxene–melt trace element partition coefficients. *Geochemistry, Geophysics, Geosystems* **15**, 303–336.

Ben Othman, D., Polvé, M. & Allègre, C. (1984). Nd–Sr isotopic composition of granulites and constraints on the evolution of the lower continental crust. *Nature* **307**, 510–515.

Bergman, S. C. (1987). Lamproites and other potassium-rich igneous rocks; a review of their occurrence, mineralogy and

geochemistry. In: Fitton, J. G. & Upton, B. G. J. (eds) *Alkaline Igneous Rocks. Geological Society, London, Special Publications* **30**, 103–190.

Bertrand, H., Dostal, J. & Dupuy, C. (1982). Geochemistry of Early Mesozoic tholeiites from Morocco. *Earth and Planetary Science Letters* **58**, 225–239.

Bizzi, L. A., De Wit, M. J., Smith, C. B., Mcdonald, I. & Armstrong, R. A. (1995). Heterogeneous enriched mantle materials and Dupal-type magmatism along the SW margin of the São Francisco craton, Brazil. *Journal of Geodynamics* **20**, 469–491.

Black, B. A. & Manga, M. (2017). Volatiles and the tempo of flood basalt magmatism. *Earth and Planetary Science Letters* **458**, 130–140.

Blackburn, T. J., Olsen, P. E., Bowring, S. A., McLean, N. M., Kent, D. V, Puffer, J., McHone, G., Rasbury, E. T. & Et-Touhami, M. (2013). Zircon U–Pb geochronology links the end-Triassic extinction with the Central Atlantic Magmatic Province. *Science* **340**, 941–945.

Blichert-Toft, J. & Albarède, F. (1997). The Lu–Hf isotope geochemistry of chondrites and the evolution of the mantle–crust system. *Earth and Planetary Science Letters* **148**, 243–258.

Boher, M., Abouchami, W., Michard, A., Albarède, F. & Arndt, N. T. (1992). Crustal growth in West Africa at 2·1 Ga. *Journal of Geophysical Research* **97**, 345–369.

Brenan, J. M., Bennett, N. R. & Zajacz, Z. (2016). Experimental results on fractionation of the highly siderophile elements (HSE) at variable pressures and temperatures during planetary and magmatic differentiation. In: Harvey, J. & Day, J. M. D. (eds) *Highly Siderophile and Strongly Chalcophile Elements in High-temperature Geochemistry and Cosmochemistry. Mineralogical Society of America and Geochemical Society, Reviews in Mineralogy and Geochemistry* **81**, 1–87.

Briden, J. C., Henthorn, D. I. & Rex, D. C. (1971). Palaeomagnetic and radiometric evidence for the age of the Freetown igneous complex, Sierra Leone. *Earth and Planetary Science Letters* **12**, 385–391.

Burke, K. & Webb, S. J. (2003). New way to map old sutures using deformed alkaline rocks and carbonatites. *Geology* **31**, 391–394.

Burke, K., Steinberger, B., Torsvik, T. H. & Smethurst, M. A. (2008). Plume generation zones at the margins of Large Low Shear Velocity Provinces on the core–mantle boundary. *Earth and Planetary Science Letters* **265**, 49–60.

Callegaro, S., Marzoli, A., Bertrand, H., Chiaradia, M., Reisberg, L., Meyzen, C., Bellieni, G., Weems, R. E. & Merle, R. (2013). Upper and lower crust recycling in the source of CAMP basaltic dykes from southeastern North America. *Earth and Planetary Science Letters* **376**, 186–199.

AQ9 Callegaro, S., et al. (2014). Enriched mantle source for the Central Atlantic magmatic province: New supporting evidence from southwestern Europe. *Lithos* **188**, 15–32.

Carlson, R. W., Esperanca, S. & Svisero, P. (1996). Chemical and Os isotopic study of Cretaceous potassic rocks from Southern Brazil. *Contributions to Mineralogy and Petrology* **125**, 393–405.

Carlson, R. W., Pearson, D. G. & James, D. E. (2005). Physical, chemical, and chronological characteristics of continental mantle. *Reviews of Geophysics* **43**, RG1001.

Carlson, R. W., Araujo, A. L. N., Junqueira-Brod, T. C., Gaspar, J. C., Brod, J. A., Petrinovic, I. A., Hollanda, M. H. B. M., Pimentel, M. M. & Sichel, S. (2007). Chemical and isotopic relationships between peridotite xenoliths and mafic–ultrapotassic rocks from Southern Brazil. *Chemical Geology* **242**, 418–437.

Castillo, P. (1988). The Dupal anomaly as a trace of the upwelling lower mantle. *Nature* **336**, 667–670.

Chakraborty, S. (2010). Diffusion coefficients in olivine, wadsleyite and ringwoodite. In: Zhang, Y. & Cherniak, D. J. (eds) *Diffusion in Minerals and Melts. Mineralogical Society of America and Geochemical Society, Reviews in Mineralogy and Geochemistry* **72**, 603–635.

Chalapathi Rao, N. V., Creaser, R., Lehmann, B. & Panwar, B. K. (2013). Re–Os isotope study of Indian kimberlites and lamproites: Implications for mantle source regions and cratonic evolution. *Chemical Geology* **353**, 36–47.

Chalokwu, C. I. (2001). Petrology of the Freetown layered complex, Sierra Leone: part II. Magma evolution and crystallisation conditions. *Journal of African Earth Science* **32**, 519–540.

Chalokwu, C. I., Seney, P. J., Wurie, C. A. & Bersch, M. (1995). Petrology of the Freetown layered complex of Sierra Leone: Part I. Stratigraphy and mineral-chemical evidence for multiple magma injection. *International Geology Review* **37**, 230–253.

Chalokwu, C. I., Ripley, E. M. & Park, Y. R. (1999). Oxygen isotopic systematics of an open-system magma chamber: an example from the Freetown Layered Complex of Sierra Leone. *Geochimica et Cosmochimica Acta* **63**, 675–685.

Chauvel, C., Lewin, E., Carpentier, M., Arndt, N. T. & Marini, J.-C. (2008). Role of recycled oceanic basalt and sediment in generating the Hf–Nd mantle array. *Nature Geoscience* **1**, 64–67.

Cherniak, D. J. (2010). Diffusion in accessory minerals: zircon, titanite, apatite, monazite and xenotime. In: Zhang, Y. & Cherniak, D. J. (eds) *Diffusion in Minerals and Melts. Mineralogical Society of America and Geochemical Society, Reviews in Mineralogy and Geochemistry* **72**, 827–869.

Choukroun, M., O'Reilly, S. Y., Griffin, W. L., Pearson, N. J. & Dawson, J. B. (2005). Hf isotopes of MARID (mica–amphibole–rutile–ilmenite–diopside) rutile trace metasomatic processes in the lithospheric mantle. *Geology* **33**, 45–48.

Class, C. & Le Roex, A. (2011). South Atlantic DUPAL anomaly—Dynamic and compositional evidence against a recent shallow origin. *Earth and Planetary Science Letters* **305**, 92–102.

Cochrane, R., Spikings, R. A., Chew, D., Wotzlaw, J.-F., Chiaradia, M., Tyrell, S., Schaltegger, U. & Van der Lelij, R. (2014). High temperature (>350 °C) thermochronology and mechanisms of Pb loss in apatite. *Geochimica et Cosmochimica Acta* **127**, 39–56.

Cohen, R. S., O'Nions, R. K. & Dawson, J. B. (1984). Isotope geochemistry of xenoliths from East Africa: implications for development of mantle reservoirs and their interaction. *Earth and Planetary Science Letters* **68**, 209–220.

Coleman, D. S., Gray, W. & Glazner, A. F. (2009). Rethinking the emplacement and evolution of zoned plutons: Geochronologic evidence for incremental assembly of the Tuolumne Intrusive Suite, California. *Geology* **32**, 433–436.

Coltorti, M., Bonadiman, C., O'Reilly, S. Y., Griffin, W. L. & Pearson, N. J. (2010). Buoyant ancient continental mantle embedded in oceanic lithosphere (Sal Island, Cape Verde Archipelago). *Lithos* **120**, 223–233.

Comin-Chiaramonti, P., Cundari, A., Piccccirillo, E. M., Gomes, C. B., Castorina, F., Censi, P., De Min, A., Marzoli, A., Speziale, S. & Velázquez, V. F. (1997). Potassic and sodic igneous rocks from Eastern Paraguay: their origin from the lithospheric mantle and genetic relationships with the associated Paraná flood tholeiites. *Journal of Petrology* **38**, 495–528.

Comin-Chiaramonti, P., de Barros Gomes, C., Cundari, A., Castorina, F. & Censi, P. (2007). A review of carbonatitic

magmatism in the Paraná–Angola–Namibia (PAN) system. *Periodico di Mineralogia* **76**, 2–3, 25.

Costa, F. & Chakraborty, S. (2004). Decadal time gaps between mafic intrusion and silicic eruption obtained from chemical zoning patterns in olivine. *Earth and Planetary Science Letters* **227**, 517–530.

Costa, F., Chakraborty, S. & Dohmen, R. (2003). Diffusion coupling between trace and major elements and a model for calculation of magma residence times using plagioclase. *Geochimica et Cosmochimica Acta* **67**, 2189–2200.

Dale, C. W., Pearson, D. G., Starkey, N. A., Stuart, F. M., Ellam, R. M., Larsen, L. M., Fitton, J. G. & Macpherson, C. G. (2009). Osmium isotopes in Baffin Island and West Greenland picrites: Implications for the $^{187}Os/^{188}Os$ composition of the convecting mantle and the nature of high $^{3}He/^{4}He$ mantle. *Earth and Planetary Science Letters* **278**, 267–277.

Davies, J. H. F. L., Marzoli, A., Bertrand, H., Youbi, N., Ernesto, M. & Schaltegger, U. (2017). End-Triassic mass extinction started by intrusive CAMP activity. *Nature Communications* **8**, 1–8.

Deckart, K., Féraud, G. & Bertrand, H. (1997). Age of Jurassic continental tholeiites of French Guyana, Surinam and Guinea: implications for the initial opening of the Central Atlantic Ocean. *Earth and Planetary Science Letters* **150**, 205–220.

Deckart, K., Bertrand, H. & Liégeois, J.-P. (2005). Geochemistry and Sr, Nd, Pb isotopic composition of the Central Atlantic Magmatic Province (CAMP) in Guyana and Guinea. *Lithos* **82**, 289–314.

De Min, A., Piccirillo, E. M., Marzoli, A., Bellieni, G., Renne, P. R., Ernesto, M. & Marques, L. (2003). The Central Atlantic Magmatic Province (CAMP) in Brazil: Petrology, geochemistry, $^{40}Ar/^{39}Ar$ ages, paleomagnetism and geodynamic implications. In: Hames, W. E., McHone, J. G., Renne, P. R. & Ruppel, C. (eds) *The Central Atlantic Magmatic Province: Insights from Fragments of Pangea. American Geophysical Union, Geophysical Monographs* **136**, 209–226.

De Paolo, D. J. (1981). Trace element and isotopic effects of combined wall-rock assimilation and fractional crystallization. *Earth and Planetary Science Letters* **53**, 189–202.

Dodson, M. H. (1973). Closure temperature in cooling geochronological and petrological systems. *Contributions to Mineralogy and Petrology* **40**, 259–274.

Douglass, J., Schilling, J.-G. & Fontignie, D. (1999). Plume–ridge interactions of the Discovery and Shona mantle plumes with the southern Mid-Atlantic Ridge (40°–55°S). *Journal of Geophysical Research* **104**, 2941–2962.

Dunning, G. R. & Hodych, J. P. (1990). U/Pb zircon and baddeleyite ages for the Palisades and Gettysburg sills of the northeastern United States: Implications for the age of the Triassic/Jurassic boundary. *Geology* **18**, 795–798.

Dupré, B. & Allègre, C. J. (1983). Pb–Sr isotope variation in Indian Ocean basalts and mixing phenomena. *Nature* **303**, 142–146.

Dupuy, C., Marsh, J., Dostal, J., Michard, A. & Testa, S. (1988). Asthenospheric and lithospheric sources for Mesozoic dolerites from Liberia (Africa): trace element and isotopic evidence. *Earth and Planetary Science Letters* **87**, 100–110.

Ellam, R. M. & Cox, K. G. (1991). An interpretation of Karoo picrite basalts in terms of interaction between asthenospheric magmas and the mantle lithosphere. *Earth and Planetary Science Letters* **105**, 330–342.

Escrig, S., Capmas, F., Dupré, B. & Allègre, C. J. (2004). Osmium isotopic constraints on the nature of the DUPAL anomaly from Indian mid-ocean-ridge basalts. *Nature* **431**, 59–63.

Escrig, S., Doucelance, R., Moreira, M. & Allègre, C. J. (2005). Os isotope systematics in Fogo Island: evidence for lower continental crust fragments under the Cape Verde Southern Islands. *Chemical Geology* **219**, 93–113.

Fraser, K. J., Hawkesworth, C. J., Erlank, A. J., Mitchell, R. H. & Scott-Smith, B. H. (1985). Sr, Nd and Pb isotope and minor element geochemistry of lamproites and kimberlites. *Earth and Planetary Science Letters* **76**, 57–70.

Gao, S., et al. (2008). Recycling deep cratonic lithosphere and generation of intraplate magmatism in the North China Craton. **270**, 41–53.

Gibson, S. A., Thompson, R. N., Dickin, A. P. & Leonardos, O. H. (1995). High-Ti and low-Ti mafic potassic magmas: Key to plume–lithosphere interactions and continental flood-basalt genesis. *Earth and Planetary Science Letters* **136**, 149–165.

Gibson, S. A., Thompson, R. N., Day, J. A., Humphris, S. E. & Dickin, A. P. (2005). Melt-generation processes associated with the Tristan mantle plume: Constraints on the origin of EM-1. *Earth and Planetary Science Letters* **237**, 744–767.

Goldstein, S. L., Soffer, G., Langmuir, C. H., Lehnert, K. A., Graham, D. W. & Michael, P. J. (2008). Origin of a 'Southern Hemisphere' geochemical signature in the Arctic upper mantle. *Nature* **453**, 89–94.

Griffin, W. L., Pearson, N. J., Belousova, E., Jackson, S. E., Van Achterbergh, E., O'Reilly, S. Y. & Shee, S. R. (2000). The Hf isotope composition of cratonic mantle: LAM-MC-ICPMS analysis of zircon megacrysts in kimberlites. *Geochimica et Cosmochimica Acta* **64**, 133–147.

Hanan, B. B. & Graham, D. W. (1996). Lead and helium isotope evidence from oceanic basalts for a common deep source of mantle plumes. *Science* **272**, 991–995.

Hanan, B. B., Blichert-Toft, J., Pyle, D. G. & Christie, D. M. (2004). Contrasting origins of the upper mantle revealed by hafnium and lead isotopes from the Southeast Indian Ridge. *Nature* **432**, 91–94.

Hargraves, R. B., Briden, J. C. & Daniels, B. A. (1999). Palaeomagnetism and magnetic fabric in the Freetown. *Geophysical Journal International* **136**, 705–713.

Hart, S. R. (1984). A large-scale isotope anomaly in the Southern Hemisphere mantle. *Nature* **309**, 753–757.

Hart, S. R., Hauri, E. H., Oschmann, L. A. & Whitehead, J. A. (1992). Mantle plumes and entrainment—Isotopic evidence. *Science* **256**, 517–520.

Hattori, K., Cabri, L. J. & Hart, S. R. (1991). Osmium isotope ratios of PGM grains associated with the Freetown Layered Complex, Sierra Leone, and their origin. *Contributions to Mineralogy and Geochemistry* **109**, 10–18.

Heinonen, J. S., Luttinen, A. V. & Bohrson, W. A. (2016). Enriched continental flood basalts from depleted mantle melts: modeling the lithospheric contamination of Karoo lavas from Antarctica. *Contributions to Mineralogy and Petrology* **171**, 1–22.

Hofmann, A. W. (2003). Sampling mantle heterogeneity through oceanic basalts: Isotopes and trace elements. In: Carlson, R. W. (ed.) *Treatise on Geochemistry—The Mantle and the Core*. Elsevier, pp. 61–101.

Jennings, E. S., Gibson, S. A., Maclennan, J. & Heinonen, J. S. (2017). Deep mixing of mantle melts beneath continental flood basalt provinces: Constraints from olivine-hosted melt inclusions in primitive magmas. *Geochimica et Cosmochimica Acta* **196**, 36–57.

Jourdan, F., Féraud, G., Bertrand, H., Watkeys, M. K., Kampunzu, A. B. & Le Gall, B. (2006). Basement control on dyke distribution in Large Igneous Provinces: Case study of the Karoo triple junction. *Earth and Planetary Science Letters* **241**, 307–322.

Jourdan, F., Bertrand, H., Schärer, U., Blichert-Toft, J., Féraud, G. & Kampunzu, B. (2007). Major and trace element and Sr, Nd, Hf, and Pb isotope compositions of the Karoo large igneous province, Botswana–Zimbabwe: lithosphere vs mantle plume contribution. *Journal of Petrology* **48**, 1043–1077.

Kamenetsky, V. S., Maas, R., Sushchevskaya, N. M., Norman, M. D., Cartwright, I. & Peyve, A. A. (2001). Remnants of Gondwanan continental lithosphere in oceanic upper mantle: Evidence from the South Atlantic Ridge. *Geology* **29**, 243–246.

Kaminsky, F. V., Sablukov, S. M., Sablukova, L. I. & Der Channer, D. M. (2004). Neoproterozoic 'anomalous' kimberlites of Guaniamo, Venezuela: mica kimberlites of 'isotopic transitional' type. *Lithos* **76**, 565–590.

Kononova, V. A., Bogatikov, O. A. & Kondrashov, I. A. (2011). Kimberlites and lamproites: criteria for similarity and differences. *Petrology* **19**, 35–55.

Korenaga, J. (2004). Mantle mixing and continental breakup magmatism. *Earth and Planetary Science Letters* **218**, 463–473.

Krause, D. C. (1963). Seaward extension and origin of the Freetown layered basic complex of Sierra Leone. *Nature* **200**, 1280–1281.

Le Roex, A. P. & Lanyon, R. (1998). Isotope and trace element geochemistry of Cretaceous Damaraland lamprophyres and carbonatites, northwestern Namibia: evidence for plume—lithosphere interactions. *Journal of Petrology* **39**, 1117–1146.

Liew, T. C., Milisenda, C. C. & Hofmann, A. W. (1991). Isotopic contrasts, chronology of elemental transfers and high-grade metamorphism: the Sri Lanka Highland granulites, and the Lewisian (Scotland) and Nuk (SW Greenland) gneisses. *Geologische Rundschau* **80**, 279–288.

Lustrino, M. (2005). How the delamination and detachment of lower crust can influence basaltic magmatism. *Earth-Science Reviews* **72**, 21–38.

Lytwyn, J., Burke, K. & Culver, S. (2006). The nature and location of the suture zone in the Rokelide orogen, Sierra Leone: Geochemical evidence. *Journal of African Earth Sciences* **46**, 439–454.

AQ14 Marzoli, A., et al. (2011). Timing and duration of the Central Atlantic magmatic province in the Newark and Culpeper basins, eastern U.S.A. *Lithos* **122**, 175–188.

Marzoli, A., Jourdan, F., Bussy, F., Chiaradia, M. & Costa, F. (2014). Petrogenesis of tholeiitic basalts from the Central Atlantic magmatic province as revealed by mineral major and trace elements and Sr isotopes. *Lithos* **188**, 44–59.

Mauche, R., Faure, G., Jones, L. M. & Hoefs, J. (1989). Anomalous isotopic compositions of Sr, Ar, and O in the Mesozoic diabase dikes of Liberia, West Africa. *Contributions to Mineralogy and Petrology* **101**, 12–18.

McDonough, W. F. & Sun, S.-s. (1995). The composition of the Earth. *Chemical Geology* **120**, 223–254.

Meisel, T., Walker, R. J., Irving, A. J. & Lorand, J.-P. (2001). Osmium isotopic compositions of mantle xenoliths: A global perspective. *Geochimica et Cosmochimica Acta* **65**, 1311–1323.

Merle, R., Marzoli, A., Bertrand, H., Reisberg, L., Verati, C., Zimmermann, C., Chiaradia, M., Bellieni, G. & Ernesto, M. (2011). $^{40}Ar/^{39}Ar$ ages and Sr–Nd–Pb–Os geochemistry of CAMP tholeiites from Western Maranhão basin (NE Brazil). *Lithos* **122**, 137–151.

AQ15 Merle, R., et al. (2014). Sr, Nd, Pb and Os isotope systematics of CAMP tholeiites from Eastern North America (ENA): evidence of a subduction-enriched mantle source. *Journal of Petrology* **55**, 133–180.

Meyers, S. R., Siewert, S. E., Singer, B. S., Sageman, B. B., Condon, D., Obradovich, J. D., Jicha, B. R. & Sawyer, D. A. (2012). Intercalibration of radioisotopic and astrochronologic time scales for the Cenomanian–Turonian boundary interval, Western Interior Basin, USA. *Geology* **40**, 7–10.

Meyzen, C. M., Cedex, L., Ludden, J. N., Humler, E. & Storey, M. (2005). New insights into the origin and distribution of the DUPAL isotope anomaly in the Indian Ocean mantle from MORB of the Southwest Indian Ridge. *Geochemistry, Geophysics, Geosystems* **6**, Q11K11, doi:10.1029/2005GC000979.

Meyzen, C. M., Blichert-Toft, J., Ludden, J. N., Humler, E., Mével, C. & Albarède, F. (2007). Isotopic portrayal of the Earth's upper mantle flow field. *Nature* **447**, 1069–1074.

Mgbatogu, C. C. S., Jones, S. J. W. & Clayton, B. R. (1988). An offshore geophysical survey of the Freetown igneous complex, Sierra Leone. *Tectonophysics* **148**, 105–114.

Mirnejad, H. & Bell, K. (2006). Origin and source evolution of the Leucite Hills lamproites: Evidence from Sr–Nd–Pb–O isotopic compositions. *Journal of Petrology* **47**, 2463–2489.

Mitchell, R. H. & Bergman, S. C. (1991). *Petrology of Lamproites*. Plenum, 447 pp.

Murphy, D. T., Collerson, K. D. & Kamber, B. S. (2002). Lamproites from Gaussberg, Antarctica: possible Transition Zone melts of Archaean subducted sediments. *Journal of Petrology* **43**, 981–1001.

Nelson, D. R. (1992). Isotopic characteristics of potassic rocks; evidence for the involvement of subducted sediments in magma genesis. *Lithos* **28**, 403–420.

Nowell, G. M., Pearson, D. G. & Irving, A. J. (2003). Lu–Hf and Re–Os systematics of lamproites: constraints on their petrogenesis. *Geophysical Research Abstracts*, 05458. AQ16

O'Brien, H. E., Irving, A. J., McCallum, I. S. & Thirlwall, M. F. (1995). Strontium, neodymium, and lead isotopic evidence for the interaction of post-subduction asthenospheric potassic mafic magmas of the Highwood Mountains, Montana, USA, with ancient Wyoming craton lithospheric mantle. *Geochimica et Cosmochimica Acta* **59**, 4539–4556.

O'Reilly, S. Y., Zhang, M., Griffin, W. L., Begg, G. & Hronsky, J. (2009). Ultradeep continental roots and their oceanic remnants: A solution to the geochemical 'mantle reservoir' problem? *Lithos* **112**, 1043–1054.

Papike, J. J., Cameron, K. L. & Baldwin, K. (1974). Amphiboles and pyroxenes: characterization of other than quadrilateral components and estimates of ferric iron from microprobe data. *Geological Society of America, Abstracts with Programs* **6**, 1053–1054.

Peate, D. W., Hawkesworth, C. J., Mantovani, M. M. S., Rogers, N. W. & Turner, S. P. (1999). Petrogenesis and stratigraphy of the high-Ti/Y Urubici magma type in the Parana Flood Basalt Province and implications for the nature of 'Dupal'-type mantle in the South Atlantic region. *Journal of Petrology* **40**, 451–473.

Pouclet, A., Allialy, M., Daouda-Yao, B. & Esso, B. (2004). Découverte d'un diatrème de kimberlite diamantifère à Séguéla en Côte-d'Ivoire. *Comptes Rendus: Géoscience* **336**, 9–17.

Prelević, D., Stracke, A., Foley, S. F., Romer, R. L. & Conticelli, S. (2010). Hf isotope compositions of Mediterranean lamproites: Mixing of melts from asthenosphere and crustally contaminated mantle lithosphere. *Lithos* **119**, 297–312.

Puffer, J. H. (2001). Contrasting high field strength element contents of continental flood basalts from plume versus reactivated-arc sources. *Geology* **29**, 675–678.

Puffer, J. H. (2003). A reactivated back-arc source for CAMP magma. In: Hames, W. E., McHone, J. G., Renne, P. R. & Ruppel, C. (eds) *The Central Atlantic Magmatic Province:*

Insights from Fragments of Pangea. American Geophysical Union, Geophysical Monographs **136**, 151–161.

Puffer, J. H., Block, K. A. & Steiner, J. C. (2009). Transmission of flood basalts through a shallow crustal sill and the correlations of the sill layers with extrusive flows: the Palisades intrusive system and the basalts of the Newark Basin, New Jersey, U.S.A. *Journal of Geology* **117**, 139–155.

Regelous, M., Niu, Y., Abouchami, W. & Castillo, P. R. (2009). Shallow origin for South Atlantic Dupal Anomaly from lower continental crust: Geochemical evidence from the Mid-Atlantic Ridge at 26° S. *Lithos* **112**, 57–72.

Rekhämper, M. & Hofmann, A. W. (1997). Recycled ocean crust and sediment in Indian Ocean MORB. *Earth and Planetary Science Letters* **147**, 93–106.

Renne, P. R., Mundil, R., Balco, G., Min, K. & Ludwig, K. R. (2010). Joint determination of ^{40}K decay constants and ^{40}Ar*/^{40}K for the Fish Canyon sanidine standard, and improved accuracy for ^{40}Ar/^{39}Ar geochronology. *Geochimica et Cosmochimica Acta* **74**, 5349–5367.

Renne, P. R., Balco, G., Ludwig, K. R., Mundil, R. & Min, K. (2011). Response to the comment by W. H. Schwarz *et al.* on 'Joint determination of ^{40}K decay constants and ^{40}Ar*/^{40}K for the Fish Canyon sanidine standard, and improved accuracy for ^{40}Ar/^{39}Ar geochronology' by P. R. Renne *et al.* (2010). *Geochimica et Cosmochimica Acta* **75**, 5097–5100.

Renne, P. R., Deino, A. L., Hilgen, F. J., Kuiper, K. F., Mark, D. F., Mitchell, W. S., III, Morgan, L. E., Mundil, R. & Smit, J. (2013). Time scales of critical events around the Cretaceous–Paleogene boundary. *Science* **339**, 684–687.

Rioux, M., Bowring, S. A., Dudas, F. & Hanson, R. (2010). Characterizing the U–Pb systematics of baddeleyite through chemical abrasion: application of multi-step digestion methods to baddeleyite geochronology. *Contributions to Mineralogy and Petrology* **160**, 777–801.

Ripley, E. M., Lightfoot, P. C., Li, C. & Elswick, E. R. (2003). Sulfur isotopic studies of continental flood basalts in the Noril'sk region: Implications for the association between lavas and ore-bearing intrusions. *Geochimica et Cosmochimica Acta* **67**, 2805–2817.

Rocha-Júnior, E. R. V., Puchtel, I. S., Marques, L. S., Walker, R. J., Machado, F. B., Nardy, A. J. R., Babinski, M. & Figueiredo, A. M. G. (2012). Re–Os isotope and highly siderophile element systematics of the Paraná continental flood basalts (Brazil). *Earth and Planetary Science Letters* **337–338**, 164–173.

Rocha-Júnior, E. R. V., Marques, L. S., Babinski, M., Nardy, A. J. R., Figueiredo, A. M. G. & Machado, F. B. (2013). Sr–Nd–Pb isotopic constraints on the nature of the mantle sources involved in the genesis of the high-Ti tholeiites from northern Paraná Continental Flood Basalts (Brazil). *Journal of South American Earth Sciences* **46**, 9–25.

Roeder, P. L. & Emslie, R. F. (1970). Olivine–liquid equilibrium. *Contributions to Mineralogy and Petrology* **29**, 275–289.

Rotenberg, E., Davis, D. W., Amelin, Y., Ghosh, S. & Bergquist, B. A. (2012). Determination of the decay-constant of ^{87}Rb by laboratory accumulation of ^{87}Sr. *Geochimica and Cosmochimica Acta* **85**, 41–57.

Ruiz-Martínez, V. C., Torsvik, T. H., Van Hinsbergen, D. J. J. & Gaina, C. (2012). Earth at 200 Ma: Global palaeogeography refined from CAMP palaeomagnetic data. *Earth and Planetary Science Letters* **331–332**, 67–79.

Saal, E., Rudnick, R. L., Ravizza, G. E. & Hart, S. R. (1998). Re–Os isotope evidence for the composition, formation and age of the lower continental crust. *Nature* **393**, 58–61.

Salters, V. J. M. & Sachi-Kocher, A. (2010). An ancient metasomatic source for the Walvis Ridge basalts. *Chemical Geology* **273**, 151–167.

Salters, V. J. M., Ragland, P. C., Hames, W. E., Milla, K. & Ruppel, C. (2003). Temporal chemical variations within lowermost Jurassic tholeiitic magmas of the Central Atlantic Magmatic Province. In: Hames, W. E., McHone, J. G., Renne, P. R. & Ruppel, C. (eds) *The Central Atlantic Magmatic Province: Insights from Fragments of Pangea. American Geophysical Union, Geophysical Monographs* **136**, 163–177.

Schoene, B., Guex, J., Bartolini, A., Schaltegger, U. & Blackburn, T. J. (2010). Correlating the end-Triassic mass extinction and flood basalt volcanism at the 100 ka level. *Geology* **38**, 387–390.

Schwindrofska, A., Hoernle, K., Hauff, F., van den Bogaard, P., Werner, R. & Garbe-Schönberg, D. (2016). Origin of enriched components in the South Atlantic: Evidence from 40 Ma geochemical zonation of the Discovery Seamounts. *Earth and Planetary Science Letters* **441**, 167–177.

Shirey, S. B. & Walker, R. J. (1998). The Re-Os isotope system in cosmochemistry and high-temperature geochemistry. *Annual Reviews in Earth and Planetary Science* **26**, 423–500.

Skinner, E. M. W., Apter, D. B., Morelli, C. & Smithson, N. K. (2004). Kimberlites of the Man craton, West Africa. *Lithos* **76**, 233–259.

Smith, M. E., Chamberlain, K. R., Singer, B. S. & Carroll, A. R. (2010). Eocene clocks agree: coeval ^{40}Ar/^{39}Ar, U–Pb and astronomical ages from the Green River Formation. *Geology* **38**, 527–530.

Stracke, A., Hofmann, A. W. & Hart, S. R. (2005). FOZO, HIMU, and the rest of the mantle zoo. *Geochemistry, Geophysics, Geosystems* **6**, Q05007, doi:10.1029/2004GC000824.

Sun, S.-s. & McDonough, W. F. (1989). Chemical and isotopic systematics of oceanic basalts: implications for mantle composition and processes. In: Saunders, A. D. & Norry, M. J. (eds) *Magmatism in the Ocean Basins.* Geological Society, London, Special Publications **42**, 313–345.

Svensen, H. H., Torsvik, T. H., Callegaro, S., Augland, L. E., Heimdal, T. H., Jerram, D. A., Planke, S. & Pereira, E. (2017). Gondwana Large Igneous Provinces: Plate reconstructions, volcanic basins and sill volumes. In: Sensarma, A. & Storey, B. C. (eds) *Large Igneous Provinces from Gondwana and Adjacent Regions. Geological Society, London, Special Publications* **463** (in press).

Taylor, W. R., Tompkins, L. A. & Haggerty, S. E. (1994). Comparative geochemistry of West African kimberlites: evidence for a micaceous end member of sublithospheric origin. *Geochimica et Cosmochimica Acta* **58**, 4011–4037.

Tegner, C., Wilson, J. R. & Robins, B. (2005). Crustal contamination in basalt and jotunite: constraints from layered intrusions. *Lithos* **83**, 299–316.

Tibbetts, N. J. (2010). The mantle xenolith perspective on trace element partitioning, oxygen fugacity and isotope systematics of subducted oceanic lithosphere. Electronic Theses, Treatises and Dissertations, Paper 4632.

Torsvik, T. H., Burke, K., Steinberger, B., Webb, S. J. & Ashwal, L. D. (2010). Diamonds sampled by plumes from the core–mantle boundary. *Nature* **466**, 352–355.

Umeji, A. C. (1983). Geochemistry and mineralogy of the Freetown layered basic igneous complex of Sierra Leone. *Chemical Geology* **39**, 17–38.

Verati, C., Bertrand, H. & Féraud, G. (2005). The farthest record of the Central Atlantic Magmatic Province into West Africa craton: Precise ^{40}Ar/^{39}Ar dating and geochemistry of Taoudenni basin intrusives (northern Mali). *Earth and Planetary Science Letters* **235**, 391–407.

Vervoort, J. D., Patchett, P. J., Blichert-Toft, J. & Albarède, F. (1999). Relationships between Lu–Hf and Sm–Nd isotopic systems in the global sedimentary system. *Earth and Planetary Science Letters* **168**, 79–99.

AQ17

AQ18

Wells, M. K. (1962). Structure and petrology of the Freetown layered basic complex of Sierra Leone. *Overseas Mineralogical Resarch Bulletin Supplement* **4**, 1–115.

Wen, L. (2006). A compositional anomaly at the Earth's core–-mantle boundary as an anchor to the relatively slowly moving surface hotspots and as source to the DUPAL anomaly. *Earth and Planetary Science Letters* **246**, 138–148.

Whalen, L., Gazel, E., Vidito, C., Puffer, J., Bizimis, M., Henika, W. & Caddick, M. J. (2015). Supercontinental inheritance and its influence on supercontinental breakup: The Central Atlantic Magmatic Province and the breakup of Pangea. *Geochemistry, Geophysics, Geosystems* **16**, 3532–3554.

Workman, R. K. & Hart, S. R. (2005). Major and trace element composition of the depleted MORB mantle (DMM). *Earth and Planetary Science Letters* **231**, 53–72.

Wotzlaw, J. F., Bindeman, I. N., Schaltegger, U., Brooks, K. C., Naslund, H. R. & Gerdes, A. (2012). Zircon records crystallization, hydrothermal alteration and remelting in the Skaergaard intrusive complex. *Earth and Planetary Science Letters* **355–356**, 199–212.

Ying, J. F., Zhang, H. F. & Tang, Y. J. (2010). Lower crustal xenoliths from Junan, Shandong province and their bearing on the nature of the lower crust beneath the North China Craton. *Lithos* **119**, 363–376.

Zeh, A., Ovtcharova, M., Wilson, A. H. & Schaltegger U. (2015). The Bushveld Complex was emplaced and cooled in less than one million years—results from zirconology and tectonic implications. *Earth and Planetary Science Letters* **418**, 103–114.

Zindler, A. & Hart, S. R. (1986). Chemical geodynamics. *Annual Review of Earth and Planetary Sciences* **14**, 493–571.